A Phase-shifted Fiber Bragg Grating Based Humidity Sensor

by

Hao Wang

A thesis
presented to the University of Waterloo
in fulfillment of the
thesis requirement for the degree of
Master of Applied Science
in
Electrical and Computer Engineering

Waterloo, Ontario, Canada, 2013

AUTHOR'S DECLARATION

I hereby declare that I am the sole author of this thesis. This is a true copy of the thesis, including any required final revisions, as accepted by my examiners.

I understand that my thesis may be made electronically available to the public.

Abstract

A humidity fiber optic sensor based on phase-shifted (PS) Fiber Bragg gratings (FBG) is demonstrated. Compared to the standard FBG sensors, the peak of the PS-FBG slips into 2 narrow peaks and forms a sharp dip in the middle. As a result, the resolution of the measurement will be higher. The sensors used in the experiments were fabricated by coating the PS-FBG surface with a moisture-sensitive polyimide and is based on the strain effect caused by the swelling of the coating after moisture absorption. The same trend seen in a standard FBG sensor can be achieved, but with higher measurement resolution in environments differing by humidity and temperature. This thesis presents simulation and measurement results, including sensitivity and response time, of the PS-FBG sensor approach for humidity sensing, as compared to the standard FBG sensors. Stability and hysteresis are also discussed.

Acknowledgements

First I would like to express my sincere thanks to my supervisor Professor Dayan Ban for his good suggestions and guidance. His positive attitude to the experiment and research makes this thesis possible.

I thank Dr. George Xiao of the National Research Council of Canada for his support in accomplishing these experiments. In addition, I would like to thank Defense R&D Canada (DRDC), National Research Council Canada (NRC) and Natural Sciences and Engineering Research Council of Canada (NSERC) for the financial support of the work. Moreover, I would like to thank Dr. Sullivan and Allan Rogalsky for technical assistance with experimental instruments.

Special thanks go to my family and friends. Without their support, I could not accomplish my research and degree.

Dedication

This thesis is dedicated to my dear parents.

Table of Contents

List of Figures

List of Tables

Chapter 1
Introduction

Among the many tools, approaches, probes and sensors on the market, Fiber Bragg Gratings emerge as the preferred choice for non-intrusive multi-parameter sensing, due to their desirable characteristics including electrical passivity, immunity to electromagnetic interference, small sizes, low insertion losses, and high sensitivity [1]. Fiber Bragg Gratings (FBGs) have received more attention in the past decades due to their numerous strain [2-3], temperature [2], humidity [4-5] and acoustic [6-7] properties. Compared to other types of sensors, FBG sensors have demonstrated three major advantages. First, they produce excellent multiplexing capability (tens or hundreds of FBG sensors can be fabricated and monitored on a single optical fiber), making them suitable for sensing applications at multiple places. Second, their remote monitoring capability allows us to maintain accurate and rapid control at a distance. Third, FBGs are small and light, resulting in easily installation into small spaces without damaging the interior structure. Meanwhile, they provide good immunity to electromagnetic (EMI) and radio frequency (RFI) interference, due to their electrical insulation. Over the years, this sensor type has had its optical characteristics manipulated for different sensing mechanisms and applications.

While FBG detectors can produce numerous advantages in sensing applications, several technical problems still need to be overcome. One of the most considerable challenges is the measurement resolution, and phase-shifted FBGs are introduced into the research to address this issue. In recent years, the phase-shifted Fiber Bragg Grating (PS-FBG) filter has been explored for sensing applications [8-9]. The PS-FBG is an optical filter that transmits a very narrow line width within a much broader reflection spectrum. By introducing a π phase shift in the middle of the grating the result will be effectively two identical gratings, separated by a half wavelength. The consequence of this is the generation of two separate gratings that act as an extended Fabry-Perot etalon, which selects the transmitted wavelength. Sui P. Yam *et al.* [10] fabricated a PS-FBG by

launching an ultraviolet (UV) laser through a phase mask to develop the etalon pattern between two standard FBGs.

In this research, we report an improved Bragg wavelength resolution by PS-FBGs coated with polyimide. For the standard FBG, a wide range and approximately flat shape of spectral top makes it difficult to distinguish the peak point. However, in the centre position of the Bragg wavelength peak, the π-phase-shifted gratings yield a split into two narrow peaks and produce a sharp dip, which can be easily resolved. This provides a higher resolution and accuracy in resolving the Bragg wavelength. Taking advantage of this high-resolution fiber sensor, we discuss the sensitivity and time response, which can be influenced by temperature and humidity throughout the polyimide coating. This thesis evaluates the feasibility of fabricating humidity sensors using π-PS-FBG, and reports on the operation principle and their performances at humidity sensing. The results show better accuracy in spectrum and parallel performance against the standard FBG.

1.1 History of Fiber Optics

An optical fiber is made from glass or plastic and transmits data as light. The setup can include many threads in modern times. In the early 1840s physicists Daniel Collodon and Jacques Babinet first demonstrated that light could be directed inside a curved jet of water from a fountain, an example of the basic principal at work in fiber optics [11]. In 1880 the 'Photophone', which could transmit a voice through a light beam, was invented by Alexander Graham Bell and Sumner Tainter in Washington, D.C [12]. They focused sunlight with a mirror and then built a system that vibrated the mirror in accordance to the speaker's voice. At the receiving end, a detector received the vibrating beam and translated it back into a voice. In 1930, German medical student Heinrich Lamm was the first person to assemble a bundle of optical fibers to transmit an image [13]. In 1973 Bell Laboratories developed a modified chemical vapor deposition process that heats chemical vapors and oxygen to form ultra-transparent glass that can be mass-produced into low-loss optical fiber [14]. This process still remains the standard for fiber-optic cable manufacturing. In 1978 the photoconductive property of fibers was discovered in Ge-

doped silicon fibers, and the first in-fiber Bragg grating was demonstrated. After 11 years, in 1989, FBGs were inscribed into fiber sensors by using the UV laser [15], and this was a significant step in the fiber gratings fabrication history. In the late 1970s and early 1980s, telephone companies began to use fibers extensively to rebuild their communications infrastructure. After this, a series of the discoveries were made in the progression of optical fiber technologies. Today more than 80 percent of the world's long-distance traffic is carried over optical fiber cables, and 25 million kilometers of the cable Maurer, Keck and Schultz designed has been installed worldwide.

1.2 Advantages

Compared to traditional electrical and mechanical sensors, FBG sensors have several advantages: First, they have good immunity to electromagnetic interferences. Normally the frequency of background electromagnetic radiation is much lower than that of optical waves [16], so the optical signal will not be altered during the transmission in the fiber. Second, they are resistant to corrosion [17], as the material of fiber sensors is silicon, which has outstanding chemical stability. FBG sensors can therefore be used in extremely hot or corrosive environments. Third, conventional sensors are big and so they cannot be used in some small place like cracks. Their light weight and small size make fiber sensors more suitable [18]. The fiber sensor is also flexible to suit a crooked condition. Low insertion loss is also a significant advantage for fiber sensors replacing traditional sensors to accomplish remote monitoring [19]. Furthermore, a fiber sensor can be used to measure numerous parameters such as temperature, humidity, strain, flux, current, pressure, and solution concentration.

1.3 Applications of Fiber sensors

1.3.1 Applications in Civil Engineering

In civil engineering layout FBG sensors monitoring is very active. The measurement of mechanical parameters is very important to the protection and monitoring of bridges, mines, tunnels, dams, buildings, etc. [20][21]. By measuring the strain distribution some

of the future deformation and breakage can be predicted. Fiber sensors can be attached to the surface or pre-embedded in the structure, which can be deployed for impact detection, shape monitoring, and oscillation damping. In this case, the critical points of the structure are monitored. Multiple fiber sensors can be connected into a sensing network, and computers can survey sensor signals over long distances. For example, fiber optics sensors are widely used in the monitoring of cracks. Local deformation will lead to cracks or slips, bending the buried fiber and altering the optical waveguide reflection conditions. Consequently, optical loss is added, or the optical spectrum will change [22].

1.3.2 Application in Power Systems

In power systems, to measure temperature, current and other parameters, as in the monitoring of high voltage transformer systems, a traditional sensor is susceptible to the electromagnetic interference and so cannot be used [23]. Fiber optic sensors are necessary. Distributed optical fiber temperature sensors in recent years have developed for real-time measurement of spatial temperature distribution, because they not only have the general advantages of fiber optic sensors but can distribute sensing along the length of the fibers. Taking advantage of this feature we can continuously detect the real-time temperature of each point along the optical fiber within a few kilometers. Positioning accuracy can be to within one meter, and measurement sensitivity down to one degree centigrade is possible. Fiber optics serves as ideal sensors for temperature detection in a wide range of applications.

1.3.3 Application in Shipping, Aerospace, Medicine and Chemical Detection

Advanced composite materials can have better anti-fatigue and anti-corrosion properties, which can lead to a reduction in the weight of a hull or fuselage, and this plays a significant role in shipping and aviation [24]. Composites are increasingly being used to create aviation and aerospace engineering. When monitoring the frames of ships, aircraft or spacecraft, several parameters demand attention: deformation torque, shear stress, and deck blow force. About 100 sensors are needed on a general hull. Fiber sensors which have strong wavelength multiplexing capability are critical components for hull testing.

Moreover, in order to monitor the strain, temperature, vibration, landing controls, ultrasonic turbulence and acceleration of an airplane, the general demand is more than 100 sensors, so the weight of the sensor must be as light as possible. In addition, aircraft composites materials have anisotropic mechanical properties, and embedded FBG sensors can be also used to complete the multi-point multi-axial strain and temperature measurement. As a result, the most flexible optical fiber sensor is usually the best choice.

Fiber sensors can also be used in other areas, such as medical science [25] and chemistry [26]. One application is measuring heart rate. For this, a doctor inserts a canal embedded with the fiber sensors into the right atrium, and injects a cold solution. The temperature of the blood can be measured, and with pulse power output we can know the amount of blood in the heart, which is very important for cardiac monitoring.

Fiber sensors can also be used for chemical sensing. Since the center wavelength of the grating is controlled by the refractive index, changes in the concentration of chemicals that affect the index can be monitored. The pH and salt concentration of a solution can be established and tracked in this way.

1.4 Challenge and Research Purpose

Although fiber sensors have numerous advantages, several improvements still need to be considered. First, measurement of the wavelength drift to perceive changes in the external physical parameters by FBGs must be advanced. If we want to widen the scope of measurement, a broadband light source must be used. Improving the resolution then demands that we make the reflection line width narrow, and this greatly reduces the power efficiency of the light source. Thus, in current FBG sensing systems a broadband high-power light source must be used to get an adequate SNR.

Secondly, to sense the changes in physical parameters, we observe the wavelength shift, so we need to improve the sensitivity and the resolution of detection with a precise spectral analyzer, increasing the cost of the entire system and reducing its usefulness. Stability is also an issue with heavy on influence on fiber sensor practicality. To sense some parameter like humidity and temperature, the fiber sensors are coated with a buffer

layer, including polyimide, PMMA, polyimide, etc. This buffer layer will be exposed in the air or solution for a long time. Developing a long-lasting buffer layer is also a challenge.

Finally, we need to make the fiber sensors more practical for regular applications. Fiber optical sensors still cannot compete with conventional sensors in many settings due to high cost and their special properties.

1.5 Preview

This thesis covers a range of research in PS-FBG sensors. Chapter 1 gives an overview of fiber optic sensors including historical developments, advantages, applications, necessary improvements and the research purpose of this thesis.

Chapter 2 offers the literature and background of FBG sensors and PS-FBG sensors. The biggest merit of this phase-shift introduced in this thesis is higher measurement resolution. I will also present a polyimide coating layer which has good sensitivity to humidity and temperature. Meanwhile, the principles of the Bragg wavelength are also discussed in Chapter 2, and relationships between wavelength and several parameters, like water uptake and temperature, are introduced.

Chapter 3 contains the experiment setup and some effects of environmental conditions on the polyimide coating. A simulation showing the relationship between the wavelength variation and parameters including water uptake, fiber radius, coating thickness, temperature and humidity is established, and we also discuss the time response using Matlab, where the ascending and descending order are both illustrated.

In Chapter 4, the spectrum, humidity, temperature and time response results are presented. We also compare the uniform FBG and π-PS-FBG. The most obvious difference is that the sharp tip of the PS-FBG spectrum replaces the flat peak of the standard FBG. The comparison between the experiment results and the simulation with hysteresis are also illustrated.

In Chapter 5, we conclude and summarize the findings of the simulations and measurements, and outline the prospects for future work.

Chapter 2
Principles

2.1 Fiber Optic Sensor

In recent years, sensors have developed in the direction of greater sensitivity, precision, adaptability, compactness and intelligence. In this process the optical fiber sensor has received much attention. These fibers have many excellent properties: immunity to electromagnetic (EMI) and radio frequency (RFI) interferences, small size, light weight, water-resistance, thermal stability, corrosion-resistance and remote monitoring capability. In environments with intolerable heat or radiation levels they can play a significant role in measurement or monitoring. Consequently, modern fiber optic sensors have become replacements to the traditional electromagnetic sensors.

A fiber optic sensor can be used into two ways, either as a sensing part called the intrinsic sensor, or as a transmission line called the extrinsic sensor. Intrinsic fiber optic sensors have received attention in the past decades due to their usefulness in strain, temperature, humidity and in-line reflection sensing. Extrinsic fiber optic sensors act as a media for light transmission in countless applications.

2.2 Fiber Bragg Grating

A Fiber Bragg Grating (FBG) is a permanent, periodically index-changing structure written into the core of an optical fiber. With the development of the fiber grating sensors, many derivations have been produced, including long period fiber grating, tilted FBG, chirped fiber grating and phase-shifted fiber grating. One application of the fiber grating is to achieve the chromatic dispersion compensation in an optical fiber. The fiber is treated as a selective optical delay line, which make the transit times of different wavelengths mostly equal. In the fiber, the shorter wavelength travels faster than the longer one; accounting for this, the fiber grating is made in different segment along the grating in order to reflect different wavelengths. Before bouncing back to the input end, the shorter wavelengths have to travel by a longer route. Consequently, the shorter

wavelength is delayed to allow the longer ones to catch up, achieving simultaneous arrival.

Another widespread application of the fiber grating is use as sensing components. Since its inception, FBG has been widely used in fiber optic sensing fields. As the fiber grating sensor is insensitive to electromagnetic interference, corrosion-resistant, electrically insulated, highly sensitive and low in cost, it has been paid much attention in the FBG sensing research. Due to the resonance wavelength caused by strain and temperature sensitivities, FBG sensors are mainly used for measurement of stress, strain and temperature. The wavelength shift resulting from external parameters (temperature or stress-strain) in FBGs is the essential mechanism of action. This sensor offers high sensitivity, immunity to most interference and stability for low energy light, and it is suitable for precise and accurate measurements. FBG sensors now occupy over 40% of fiber-based materials applications. Now FBG sensors have been used in various applications, such as highways, bridges, dams, mines, airports, ships, factories, railways, oil and gas storage monitoring.

Figure 2.1 shows several types of FBGs [27]. Fig. 2.1(a) is a standard FBG. Under a phase matching, a FBG has the forward propagating mode coupled with the backward propagating mode, leading to a specific wavelength missing in the transmission spectrum. The long period fiber grating can couple the forward propagating core mode to some of the cladding mode. In a chirped fiber, each wavelength is reflected at different positions as a result of a delay time difference for different reflected wavelengths. A tilted fiber grating can couple the forward propagating core mode to the backward propagating mode both in core and cladding. A sampled fiber grating can reflect several wavelengths with equal wavelength spacing. All these types of gratings have been utilized in various types of fiber grating sensors and wavelength change interrogators.

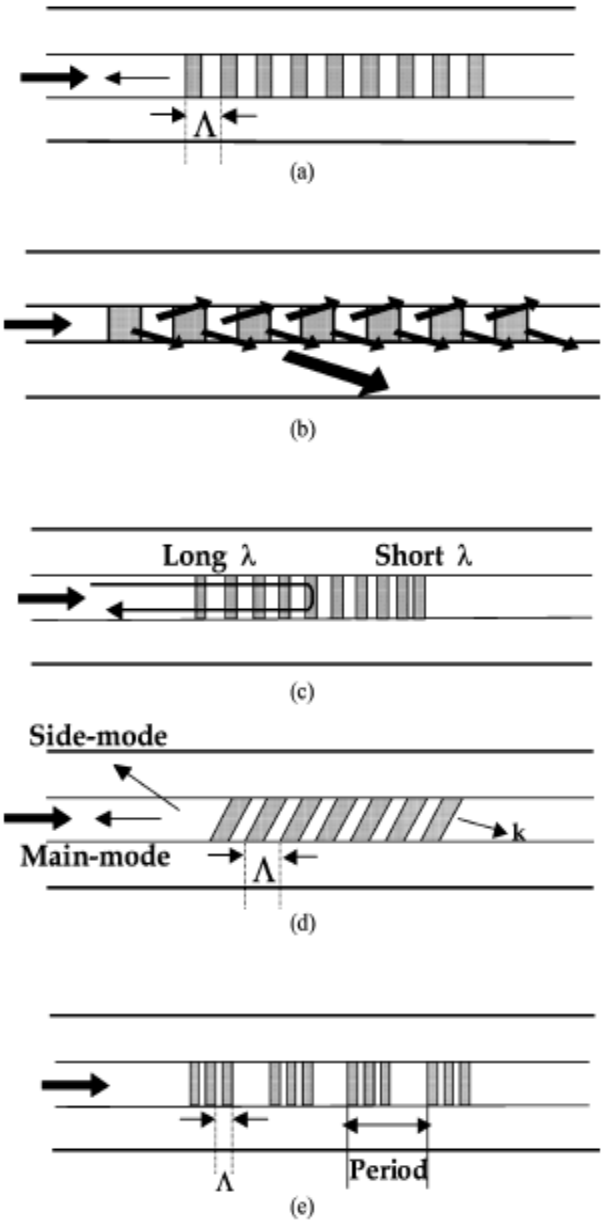

Fig. 2.1 Types of fiber Bragg gratings (a) standard FBG, (b) long period FBG, (c) chirped FBG, (d) tilted FBG, (e) sampled FBG

Many parameters, including strain, temperature and humidity, can be evaluated by FBG sensors. In 1992, Meltz and Morey demonstrated that strain and temperature changes can shift the Bragg wavelength. Due to the variation of the grating period, caused by a physical stretch and the refractive index, a shift strain was induced. Meanwhile, the

temperature response resulted from both a thermal expansion and the temperature dependence of the refractive index. Obviously, any shift of the Bragg wavelength can be taken as a result of the strain and temperature changing. The other sensing parameters, such as humidity, vibration and pressure, can be measured indirectly from considering the strain and temperature changes.

Strain is the most common factor which FBG sensors are applied to tes, and a tiny change in strain can be reliably detected for many industrial applications. Massino et al. [28] presented a field test using FBG sensors to monitor railway traffic. They demonstrated the possibility of using these FBG sensors to know train speed and acceleration with the testing of the strain track.

Temperature is one of the most significant parameters for industries and daily applications. Its measurement has been achieved by using optical fibers for decades [29], and now the current research of temperature sensing is focused on resolution and accuracy improvement and cost reduction. In 2012, Tong Sun et al. [30] developed a FBG inside a garment for monitoring a person in a dangerous environment, such as a firefighter, as astronaut or a soldier. Such data must also be used for temperature compensation during the measurement of other parameters, such as pressure and salinity.

Humidity is another critical parameter in many applications, often key in industry and weather monitoring. Furthermore, humidity is relative to temperature during testing, and compensating for temperature variation when testing the humidity is a considerable challenge [31].

Figure 2.2 shows the structure of a typical FBG sensor. As shown in Fig. 2.2, the refractive index can be adjusted with the grating period. Since light enters the core through a FBG, a part of the light will reflect while the rest will transmit through the gating. This leads to the coupling between the incoming and reflected light by the core and cladding mode. As a result, an attenuation of the light occurs at a specific wavelength, resulting in a peak in the reflection spectra as shown in Fig. 2.3 [32]. This is the Bragg wavelength. This process is demonstrated in Fig. 2.4.

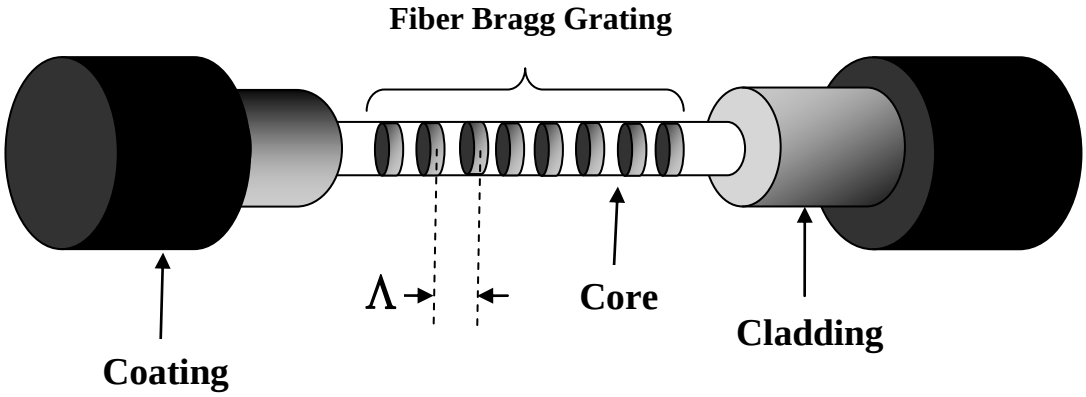

Fig. 2.2 Typical fiber Bragg grating structure

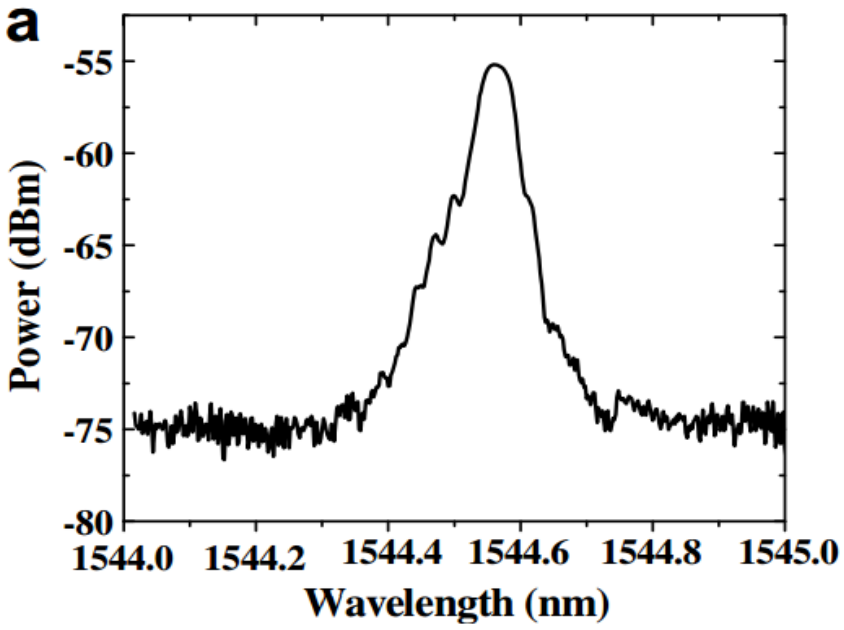

Fig. 2.3 Typical reflection spectra with Bragg wavelength

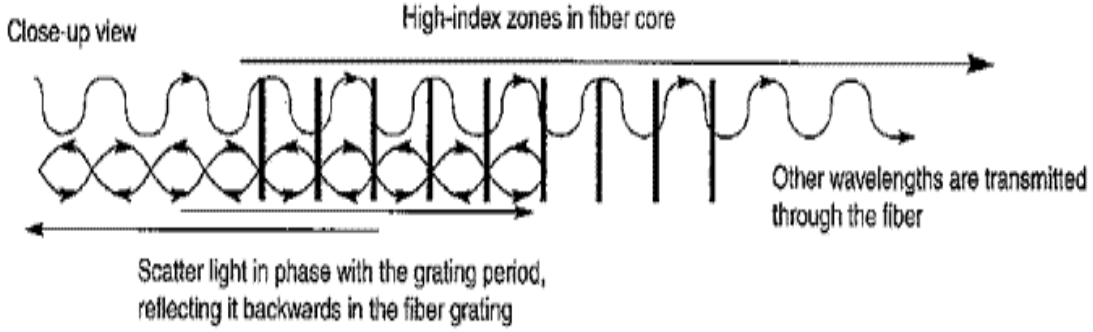

Fig. 2.4 Reflection sketch of light passing through the grating

Beyond the typical FBG structure shown in Fig. 2.2, alternate versions are possible by variation of the refractive index and grating period. The grating can be uniform, graded or distributed in a superstructure. The refractive index has two main features: index distribution and offset. Typically, the index distribution is either uniform or apodized, and the offset is positive or zero. With these two factors influencing the grating structure several categories are of interest, such as uniform positive-only index change, Gaussian apodized, aised-cosine apodized, chirped, discrete phase shift, and superstructure.

Initial experiments were carried out using a fiber sensor with a coating thickness of 33μm. This value was determined using a microscope, which yields an uncertainty of μm in the measurement. The performance of FBG sensors under variable temperature and humidity is shown by Teck L. Yeo et al. [33]. The humidity change yields a wavelength span of approximately 0.35 nm. A linear relationship between the Bragg wavelength and relative humidity was evident. The linear increase corresponds to the equations we provide above. The sensitivity of the device was estimated to be 4.5 pm/%RH at 1535 nm. Response time is a key issue which is particularly significant in applications needing very accurate data. The time taken to read before stabilization at 75%RH was found to be approximately 25 min, while the time required for the reading to move from 75%RH to ambient conditions (at 36%RH) was approximately 40 min. W. Zhang et al. [34] demonstrated polymer FBG sensors with improved response times, decreased by reducing the polymer thickness, which an important factor effect leading to different

FBG sensor performance. The RH and T sensitivities with respect to the cross-section area of the polyimide coating were observed by Kronenberg et al. [35]. They installed one bare grating and seven gratings with different average coating thicknesses. For low ratios of coating to fiber cross-section area, the fitted curves show an almost linear dependence of humidity and temperature sensitivities on cross area (S_{RH} and S_T on $A_{c)}$.

2.3 Phase-Shifted Fiber Bragg Grating

A PS-FBG is an in-fiber optical filter that transmits a very narrow line width within a much broader reflection spectrum. By introducing a π phase shift in the middle of the grating the result will in effect be two identical gratings, separated by a half wavelength. Consequently, the two separate gratings will act as an extended Fabry-Perot etalon, which can select the transmitted wavelength. Ideally, it will build one peak in the middle of the transmitted light spectrum. We usually fabricate a PS-FBG by launching a UV laser through a phase mask to develop an etalon pattern between two standard FBGs [36]. A Fabry-Perot etalon, as shown in Fig. 2.5 [37], is a tunable optical filter consisting of two parallel, highly reflecting mirrors.

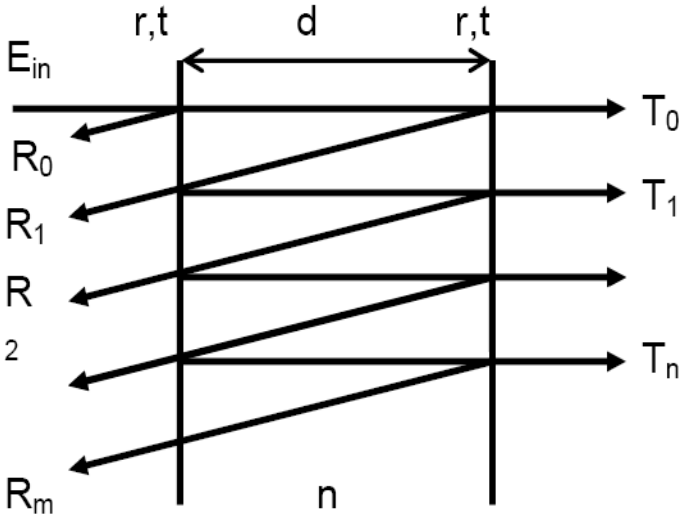

Fig. 2.5 Schematic setup of Fabry-Perot etalon

When the light enters the etalon, it will be reflected between the parallel plates several times and a small fraction will escape through the back side. As the wavelength satisfies the relationship $\lambda=2nd$, where d is the distance between the two parallel plates, the

transmitted light beams of the series T_n are all in phase while the reflected light R_m escaping from the back side will be out of phase. This leads to the constructive and destructive interference between each T and R, respectively, so light will be wholly transmitted through the filter and neighboring wavelengths will be blocked. All other wavelengths that are not in phase will simply be reflected with a small fraction that leaks through the filter. The transmitted wavelength depends on the magnitude of the phase shift. When the shift reaches a quarter of wavelength and sits in the middle of the grating there will be a small segment of the reflected spectrum that will be affected and this will open up a very narrow transmission peak in the middle of the reflection band. The whole spectrum including the peak is variable with the phase-shifted grating.

Figure 2.6 [38] illustrates a standard FBG and π PS-FBG structure. Introducing a π phase shift in the middle of the FBG results in the formation of a narrow peak with a megahertz line width. Compared to the typical width of a FBG signal of tens of GHz, the signal of a π PS-FBG is much narrower. Therefore, sensors based on PS-FBG will offer much higher resolution compared to their FBG counterparts. Indeed, high resolution strain measurement using PS-FBG has been reported recently [39-41].

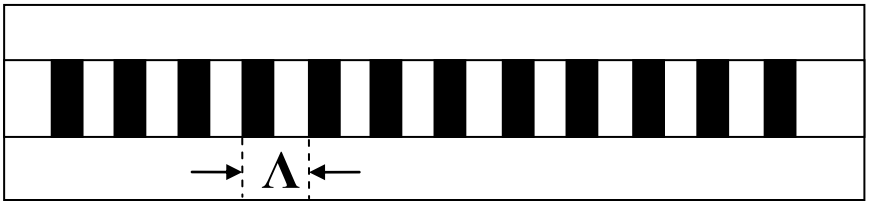

(a) Standard FBG

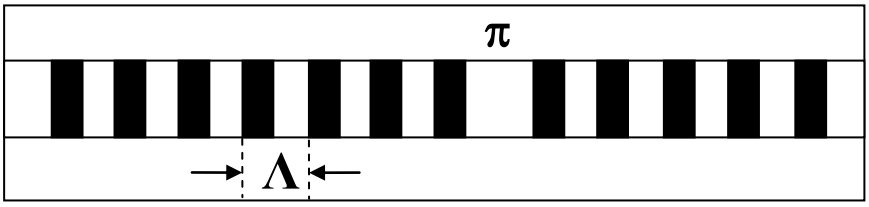

(b) π-phase shifted-FBG

Fig. 2.6 Concept of the fiber Bragg grating filters, (a) Standard FBG; (b) π-phase shifted-FBG

The position of the peak in the transmitted spectrum depends on the magnitude of the phase shift. Christophe Martinez et al. [42] did a modulation to demonstrate this relationship. As shown in Fig. 2.7, the dip exists at different positions of the transmitted spectrum due to a different phase in the standard gratings array, and with a phase shift of π it appears in the middle position. The phase-shift position is a factor that influences the shape of the transmitted spectrum. A comparison of three position values is illustrated in Fig. 2.8. δl is the distance between the phase and the middle position of the grating. Obviously, the central peak reaches different transmission values and the transmission notch decreases with increasing δl, and the transmission turns out to be the spectrum of a standard Bragg grating when the δl equals to half length of the grating.

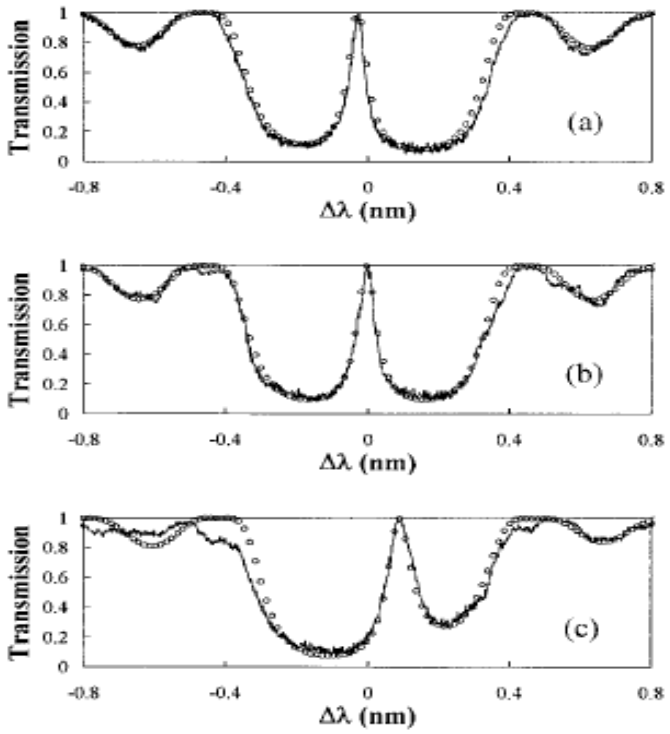

Fig. 2.7 Spectral transmission of 4-mm-long PS-FBG for three values of phase (a) π-0.25, (b) π and (c) π+1

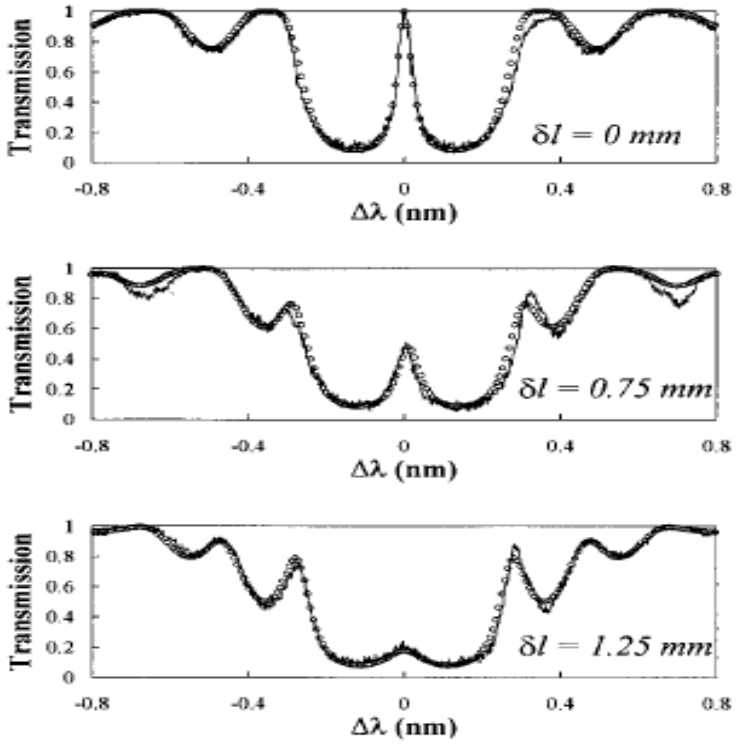

Fig. 2.8 Comparison of spectral transmissions of 4.5-mm-long π-phase-shifted FBGs for three values of the phase-shift position on the grating

2.4 Polyimide Coating

Polyimide (PI) is a polymer of imide monomers. As a result of its light weight, flexibility, thermal stability, resistance to chemical attack and excellent mechanical properties, PI is used in flexible cables, and as a stress buffer and insulating layer in electronics industries. It is one of the most reliable engineering polymers, demonstrated in its numerous applications in the packaging of electronics and fiber optics [43]. Although its moisture and temperature sensitivity is limited when compared to other polymers, PI is still treated as a common material for humidity and temperature sensing due to its unique properties. In this thesis, PI was chosen as the coating material. Most PI blends have a repeated chemical structure similar to the one shown below:

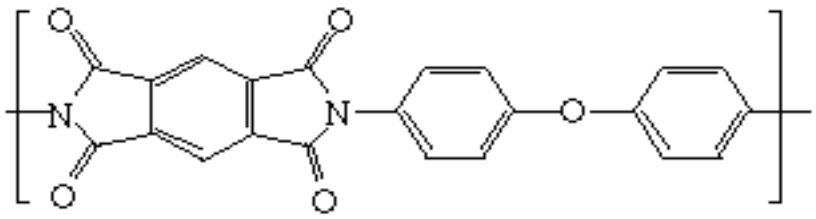

Fig. 2.9 Typical chemical structure of polyimide

This structure gives PI high temperature resistance and excellent mechanical properties, thus making it an ideal candidate for coating applications. For the π-PS-FBG humidity sensor, the PI precursor solution was coated on π-PS-FBG using a commercial optical fiber PI coater system. The thickness of the coating is controlled within 30 μm to ensure that moisture is capable of diffusing into the coating within short time period, and to ensure that the force induced by the swelling of the PI is enough to induce sufficient strain on the gratings.

When subjected to humidity or water exposure while deposited over an optical fiber sensor (e.g. FBG), the PI swells and induces strain in the grating, resulting in a wavelength shift. Figure 2.10 illustrates readings before and after humidity is induced. A thin layer of PI is coated on the fiber surface, and the swelling of the polymer produces a tensile stress on the grating, resulting in a shift of grating period and reflected wavelength. A tensile strain is induced on the fiber with pitch increasing from Λ to $\Lambda+\Delta\Lambda$, hence, the Bragg wavelength λ_B varies from $2n_{eff}\Lambda$ to $2n_{eff}(\Lambda+\Delta\Lambda)$. Therefore, the Bragg wavelength can be correlated to the humidity level. Although the moisture swelling capability of PI is not as high as that compared to other polymers, the volume expansion of the material when exposed to humidity change is linear and FBG sensors coated with PI exhibit a linear and reversible response with humidity change. Kronenberg et al. [44] reported PI-coated FBGs with different coating thickness determining the humidity and temperature responses of the sensors, and a linear and reversible response to both parameters was reported.

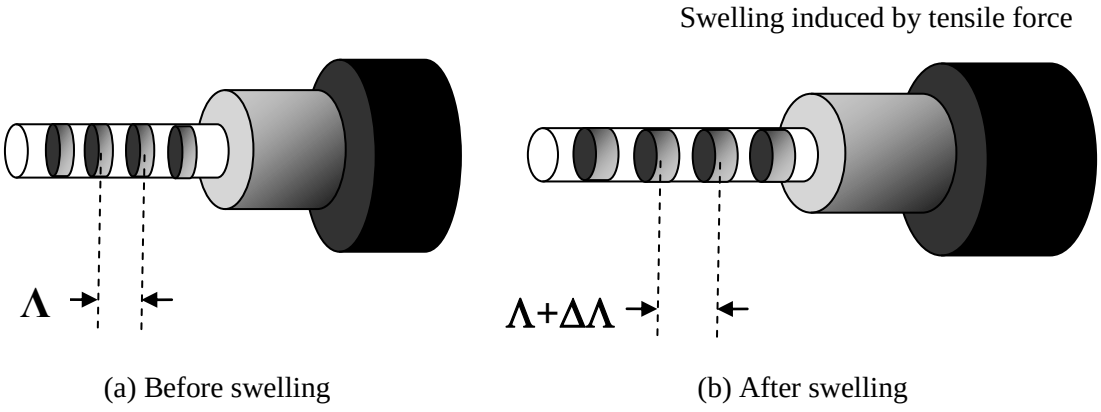

Fig. 2.10 Illustration of polymer coated FBG before and after moisture induced swelling, a period variation $\Delta\Lambda$ caused by the swelling of the PI coating, due to water absorption.

The PI we used in this thesis is PI-2525 [45], whose precursors are suitable for applications where a high temperature complicates curing. Typically these precursors are used as buffer or interlay dielectric layers on low-temperature substrates. They are easier and faster to imidize at low temperature than standard PI precursors. In the coating process, the bonding of the precursors and the substrates are completed during the softbake cycle since the highly viscous solution solidifies. All the bubbles in the solutions need time to dissipate out during this period. It is necessary to have a short delay prior to spin to allow the PI to flow, and the spin speed and time depend must be selected for a target coating thickness. After the coating a bake process, which aims to cure the PI precursor for patterning, is required. Then samples can be patterned using nanofabrication techniques with photoresist. Finally, the cure heating cycle makes the precursors convert to PI, and this requires elevated temperature and a controlled environment to accomplish the best results.

2.5 Relevant with Temperature and Humidity

As shown in Fig. 2.2, the Bragg wavelength depends on both the refractive index of the fiber core and the period of the grating. Being launched into the end of the fiber with a

FBG, the light with a specific wavelength matching the Bragg condition will reflect back, while the rest will pass through. From the Bragg grating condition, the following equation can be found:

$$2(\frac{2\pi n_{eff}}{\lambda_B}) = \frac{2\pi}{\Lambda} \tag{1}$$

The attenuated wavelength relies on the refractive index of the fiber core and the period of the gratings. As a result, the value of the Bragg wavelength is a function of the effective refractive index (n_{eff}) of the optical fiber and the grating pitch (Λ) of the FBG, which is given [46] as:

$$\lambda_B = 2n_{eff}\Lambda \tag{2}$$

As stated at the beginning of this chapter, FBGs can be used to measure the strain, temperature and humidity. For the structure shown in Fig.2.2, this is mainly caused by the coating, which can be made of silicon, PMMA, PI and so on. When the strain, temperature, humidity or other factors affect the coating, a change inside the coating occurs, and this directs a variation of the effective refractive index of the grating period, giving rise to the Bragg wavelength. Therefore, the shift in Bragg wavelength determined by the change in strain or thermal effect is given by [47]

$$\frac{\Delta\lambda_B}{\lambda_B} = (1-P_e)\varepsilon + [(1-P_e)\alpha + \xi]\Delta T \tag{3}$$

where P_e is the photoelastic constant of the fiber (the typical value for silica fiber is 0.22), ε is the strain induced on the fiber, α is the fiber thermal-expansion coefficient, and ξ is the fiber-thermooptic coefficient. The first term represents the longitudinal strain effect on the FBG and the second term represents the thermal effect, which includes thermal expansion of the material and the thermal-optic effect.

When the coating absorbs moisture, the stain ε is proportional to the moisture expansion coefficient and the relative humidity change. The shift in the Bragg wavelength for the polymer-coated FBG is given by:

$$\frac{\Delta\lambda_B}{\lambda_B} = (1-P_e)\alpha_{RH}\Delta RH + [(1-P_e)\alpha_T + \xi]\Delta T \tag{4}$$

where α_{RH} and α_T are the moisture expansion coefficient and the thermal expansion coefficient of the coated FBG, respectively. The equation can be further simplified to:

$$\frac{\Delta\lambda_B}{\lambda_B} = (1-P_e)\varepsilon_{RH} + (1-P_e)\varepsilon_T + \xi \cdot \Delta T \tag{5}$$

From the above equations, it is apparent that the shift is relative to the strain effect induced on the FBG due to moisture and to the thermal expansion and the thermooptic effect.

2.6 Relationship between Wavelength, Water Uptake and Temperature

In this section, we will introduce some parameters influencing the coating deformation: water uptake, Young's modulus, fiber radius and coating thickness. The density of the PI coating will vary after the moisture absorption. Hence, since the PI swells after the absorption of water, the density of the polymer after the absorption of the water is determined by

$$\rho'_{PI} = w\rho_{water} + (1-w)\rho_{PI} \tag{6}$$

where ρ_{water} is the density of water, ρ_{PI} is the original density of PI and w is the weight gain of the swelled PI coating. The volume expansion rate of the swelled PI can be given by

$$\frac{\Delta V}{V_0} = \frac{\rho_{PI}}{\rho'_{PI}}(w+1) - 1 \tag{7}$$

The tensile strain effect induced on the PI due to moisture and temperature is given by

$$\varepsilon_{PI} = \frac{\Delta V}{V_0}\left(1 - \frac{2D_0}{R_f + 3D_0}\right) \tag{8}$$

where D_0 is the thickness of the PI coating and R_f is the radius of the fiber. The tensile strain of the fiber is given by

$$\varepsilon_f = \frac{\sigma_f}{E_f} = \frac{F / A_f}{E_f} = \frac{\varepsilon_{PI} E_{PI} A_{PI}}{A_f E_f} \tag{9}$$

where σ is the tensile stress, f is short for fiber, PI is for the polyimide and F is the swelling force caused by the water uptake determined by the strain ε, Young's modulus E and the cross-sectional area A, which is πR^2. Eq. 10 below represents the Bragg wavelength shift for the PI coated fiber:

$$\frac{\Delta\lambda}{\lambda_B} = (1 - P_e)\varepsilon_f \tag{10}$$

where P_e is the photoelastic coefficient of the fiber, which is typically equal to 0.22 for fused silica, and λ_B is the original Bragg wavelength whose value is 1550 nm in this experiment. As a result, the Bragg wavelength change can be a function of the water uptake, coating thickness, Young's modulus and fiber radius.

Chapter 3

Simulation and Experimental Setup

3.1 Simulation

Young's modulus of glass fiber E_f	7.18E+10 N/m^2 7.32E+03 kg/mm^2
Young's modulus of Polyimide E_{PI}	3.26E+02 kg/mm2
Water Density ρ_{water}	1 g/cm^3
Polyimide Density ρ_{PI}	1.39 g/cm^3
Effective photoelastic constant for fused silica P_e	0.22

Table 1 Parameters in equations

3.1.1 Effect of the Water Absorption Rate

The water uptake is the content of the water in the PI after the absorption process. Since the moisture in the air changes the coating will absorb or release water. As the volume of water uptake can stretch of shrink the coating, the grating inside the fiber core will be grating. In this simulation, it is assumed to vary from 0 to 3.0% and the interval is set at 0.15%. Meanwhile, Table 1 shows some fixed parameter in the whole simulation. We fix the PI thickness at 30 μm. Fig. 3.1 presents the preliminary simulation results of a standard FBG at 20 water absorption points. The figure shows that the shift of the Bragg wavelength increases linearly with water uptake. From the linear curve, we obtain that higher water uptake leads to larger shift of the Bragg wavelength and higher sensitivity to humidity.

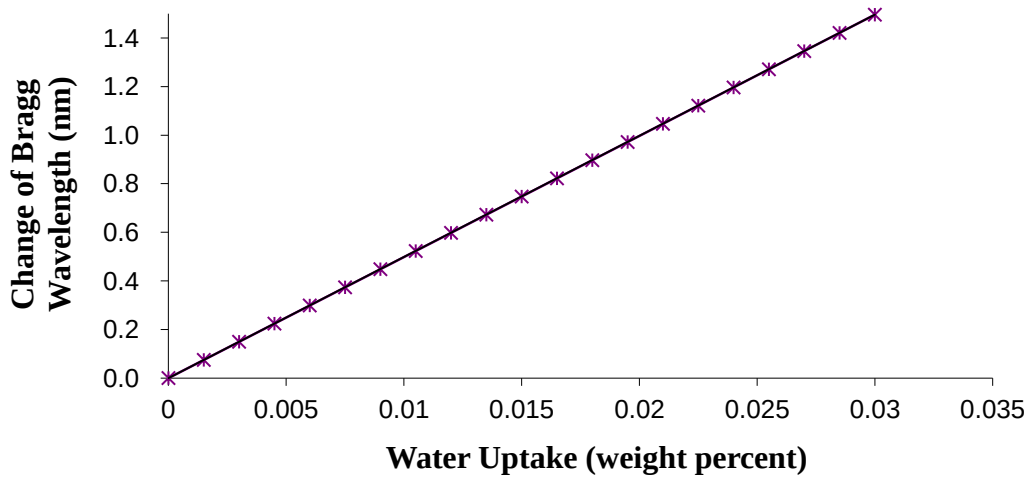

Fig. 3.1 Effect of polyimide water absorption; temperature: 85 ℃, fiber radius: 62.5μm, coating thickness: 30μm

3.1.2 Effect of the Thickness of the Polyimide Coating

We set the water uptake at 2% and the PI thickness from 2 μm to 30 μm. Fig. 3.2 shows that the change of the Bragg wavelength ascends with the increasing polyimide coating thickness approximately linearly. That means that a thicker PI coating can absorb more water and result in a larger wavelength shift and higher sensitivity. Corresponding to the experiment, PS-FBG shows a higher sensitivity than the standard FBG, resulting from the thicker coating.

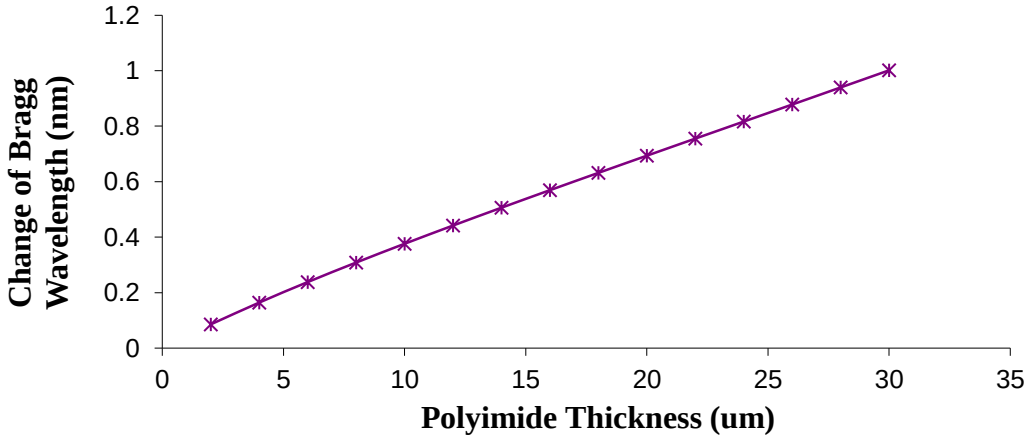

Fig. 3.2Effect of polyimide thickness; temperature: 85 ℃, fiber radius: 62.5μm, water uptake: 2%

3.1.3 Effect of Optical Fiber Radius

Besides water uptake and PI thickness, the optical fiber radius is another parameter which can impact the Bragg wavelength change. The optical fiber radius can be controlled from 42.5μm to 98.5μm with the constant water uptake at 2%. It can be seen in Fig. 3.3 that a lower fiber radius results in a smaller the change of the Bragg wavelength. Unlike the two relationships mentioned above, this curve is nonlinear as the cross-sectional area A is not proportional to the wavelength change in Eq. 9.

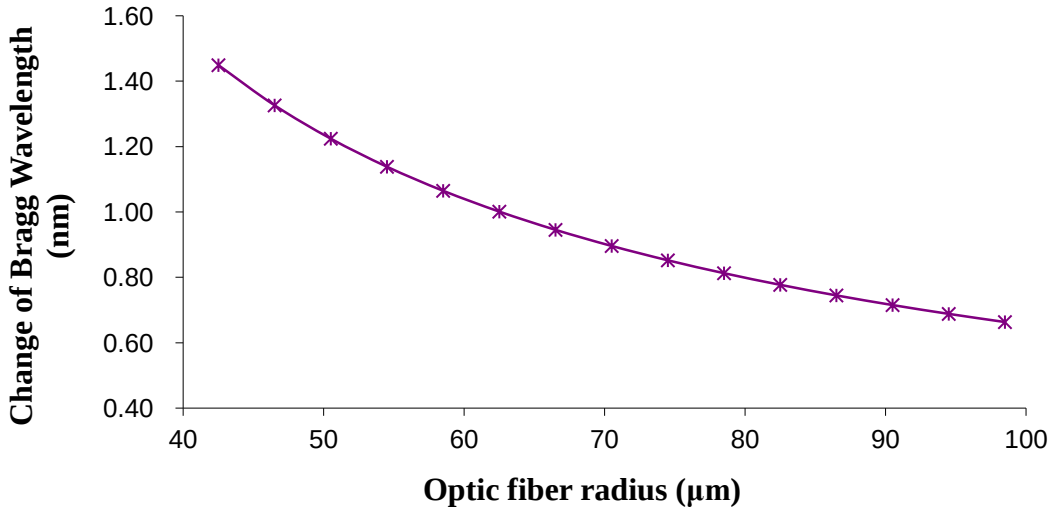

Fig. 3.3 Effect of Optical Fiber Radius; temperature: 85 ℃, water uptake: 2%, coating thickness: 30μm

3.1.4 Effect of Temperature

The variation of the Bragg wavelength depends on not only humidity but also temperature. This is caused by the change of Young's modulus at different temperatures. The relationship between the Young's modulus and temperature is given by [48]

$$E(GPa) = -0.0066T(^{\circ}C) + 5.5657 \tag{11}$$

where E is the Young's modulus of the material and T is the temperature. As shown in the Fig. 3.4, temperature is tuned from 10 ℃ to 80 ℃ and water uptake is kept at 2%. Fig. 3.4 reveals that the wavelength will linearly increase, with a smaller shift of the Bragg wavelength as the temperature rises. This is similar to the result we obtain from the

experiment. Higher temperature leads to lower sensitivity, which can be attributed to the decreasing Young's modulus.

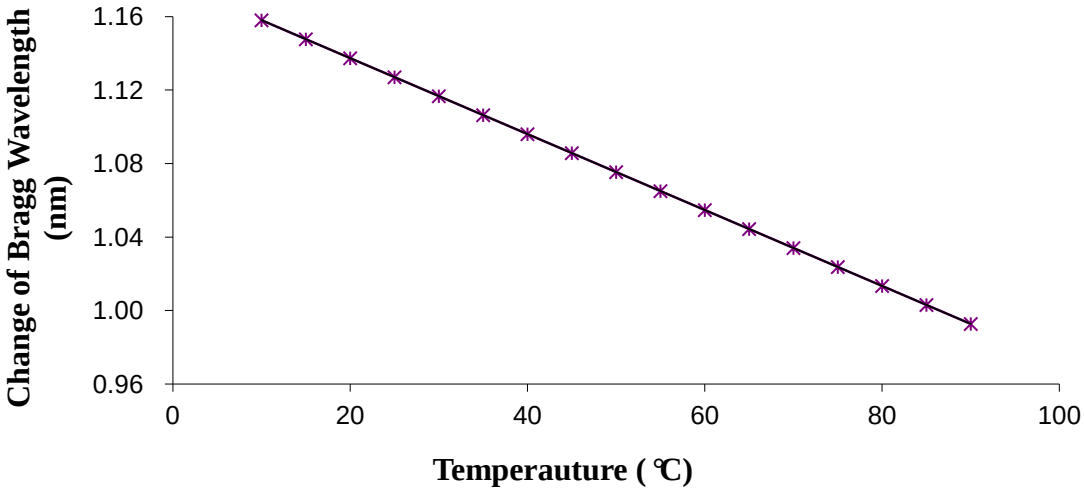

Fig. 3.4 Effect of temperature; water uptake: 2%, fiber radius: 62.5μm, coating thickness: 30μm

3.1.5 Effect of Humidity

The relationship between the humidity and water uptake is modeled by Peeyush et al. [49] by using the Guggenheim-Anderson-de-Boer equation:

$$w = M_{\infty} = \frac{M_m ACa_w}{(1 - Aa_w)(1 - Aa_w + ACa_w)} \tag{12}$$

where M_{∞} is the weight gain, a_w is the water activity, which is RH value, M_m is the monolayer moisture content, and A and C are constants related to heat of sorption. Fitting the data to Eq. 12, the coefficients were found to be M_m = 0.352 (kg water)/(kg dry basis), A = 0.28 and C = 0.18. Since the relationship between relative humidity and water uptake is not linear, the curve is not exactly linear as well. We set the humidity range from 0 to 100%. As we show in the experiment, the wavelength is increasing with the humidity change and the shift of Bragg wavelength is larger, resulting in higher sensitivity.

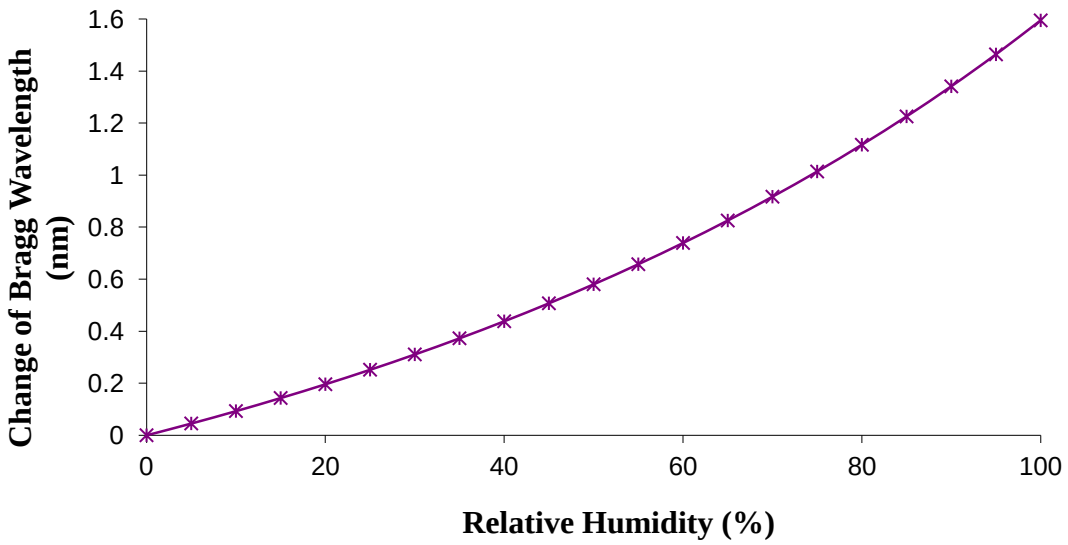

Fig. 3.5 Effect of humidity; temperature: 85 ℃, fiber radius: 62.5μm, coating thickness: 30μm

In summary, the change of the Bragg wavelength depends on several parameters such as water uptake, coating thickness, fiber radius, temperature and humidity. To increase the sensitivity of the FBG, we can try to improve the capacity of the PI coating to absorb water, increase the thickness, decrease the fiber radius or keep the fiber working in the relatively lower temperature and humidity condition.

3.1.6 Time Response

In this section, we use Matlab to model the time response of the FBG in moisture. After the change of the ambient humidity, the wavelength needs time to stabilize until the moisture saturates the PI coating. The coating is a hollow structure. Therefore, the relationship between the normalized concentration C/C_0 and time t, where C_0 is the original water concentration in the coating, is given by [50]:

$$\frac{C}{C_0} = 1 - \pi \sum_{n=1}^{\infty} \frac{J_1^2(a\alpha_n) U_0(r\alpha_n)}{J_1^2(a\alpha_n) - J_0^2(b\alpha_n)} \exp(-D\alpha_n^2 t) \qquad (13)$$

where $J_n(\cdot)$ and $Y_n(\cdot)$ are the Bessel functions of the first and second kind with the index n, a is the inner radius of the hollow structure, b is the outer radius of the hollow structure, r is the radial position, D is the diffusion coefficient, and α_n s are the positive roots of $U_0(a\alpha_n) = 0$. I set a = 62.5, b = 87, r =70 and D = 0.3μm^2;

$$U_0(r\alpha_n) = J_0(r\alpha_n)Y_0(b\alpha_n) - J_0(b\alpha_n)Y_0(r\alpha_n) \qquad (11)$$

The Matlab code is presented below.

```
maxv = 1;
maxs = 500;
b = 87;
a = 62.5;
r = 70;
q=log(r/a)/log(b/a);
bes_zero = zeros(maxv, maxs);
zero_guess = 10.1 + 0:0.1*pi:maxs*pi;
for zero_cnt = 1:length(zero_guess)-20 %% to avoid tail inaccuracies
zero_try = zero_guess(zero_cnt)/a;
bes_zero(1,zero_cnt) = fzero(@(x)besselj(0,a*x).*bessely(0,b*x)-
besselj(0,b*x).*bessely(0,a*x), zero_try);
end
bes_zero = roundn(bes_zero, -6);
bes_zero = unique(bes_zero);
figure(1)
```

```
hold on

plot(bes_zero(1:end-20), zeros(1,length(bes_zero(1:end-20))), 'or')

plot(linspace(0,bes_zero(end-20), 4000), besselj(0,a*linspace(0,bes_zero(end-20),
4000)).*bessely(0,b*linspace(0,bes_zero(end-20), 4000))-
besselj(0,b*linspace(0,bes_zero(end-20), 4000)).*bessely(0,a*linspace(0,bes_zero(end-
20), 4000)))

Ja=besselj(0,a*bes_zero);

Ur=besselj(0,r*bes_zero).*bessely(0,b*bes_zero)-
besselj(0,b*bes_zero).*bessely(0,r*bes_zero);

Jb=besselj(0,b*bes_zero);

M= Ja.*Jb.*Ur./(Ja.*Ja-Jb.*Jb);

% figure(2)

% plot(bes_zero,J1), hold on, plot(bes_zero,J3, 'r')

% plot(bes_zero,abs(J1), 'g'), hold on, plot(bes_zero,abs(J3), 'k')

c=0;

t=0:0.1:40;

for n=1:length(bes_zero)

c=c+3.14*exp(-3e-1*60*bes_zero(1,n).*bes_zero(1,n).*t) .*M(1,n);

end

c=0;

t=0:0.1:40;

for n=1:length(bes_zero)

c=c+3.14*exp(-3e-1*60*bes_zero(1,n).*bes_zero(1,n).*t) .*M(1,n);

end
```

```
c=q-c;
figure(3)
hold on
plot(t,c,'-r')
c=1-c;
plot(t,c,'-b')
xlabel('Time (min)')
ylabel('Normalized concentration');
```

Figure 3.6 illustrates the simulated time response. The red line tracks the desorption process and the blue one tracks the absorption process. From the curves in absorption and desorption rate, the sensors stabilize after approximately 10-15 minutes. However, there is still a problem for this simulation: the range of normalized concentration is to around 0.7, instead of to 1. This simulation needs an improvement.

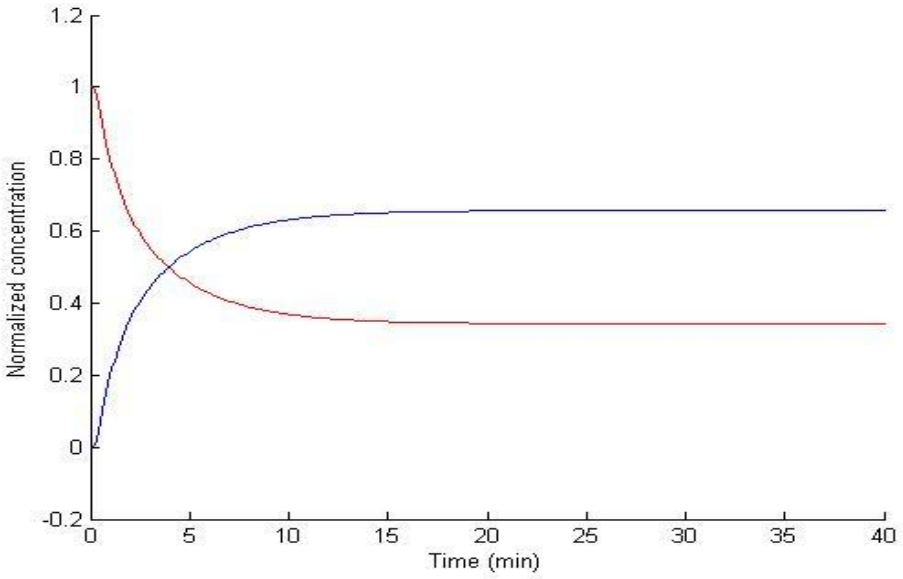

Fig. 3.6 Time response for the hollow structure of PI coating

3.2 Experiment Setup

In this chapter, we introduce a brief structure of the experiment set up, including every components. The humidity chamber is a piece of equipment able to achieve different environmental conditions. In this system, the chamber has a range of 0-100°C for temperature and 0-100% for humidity. As shown in Fig. 3.7, the fabricated FBG humidity sensor was placed in a humidity chamber in which the humidity can be tuned from 5%RH to 95%RH, and the temperature is fixed at 10°C, 30°C and 50°C. The experimental setup is illustrated in Fig. 3.7 and 3.8 including a picture and a schematic. The broad band light source in this testing system has a C-band spectrum with a range from 1525 to 1560 nm. The light enters the fiber through an optical circulator, which is a special component used to separate the signal into 2 opposite directions. By passing through the transmission port of the circulator, the reflected light from the FBG sensors is emitted into an Optical Spectrum Analyzer (OSA) where the reflection spectrum can be tested and observed in order to get the wavelength shift of the FBG sensors in different environmental conditions. Figure 3.8 shows a picture of the measurement system.

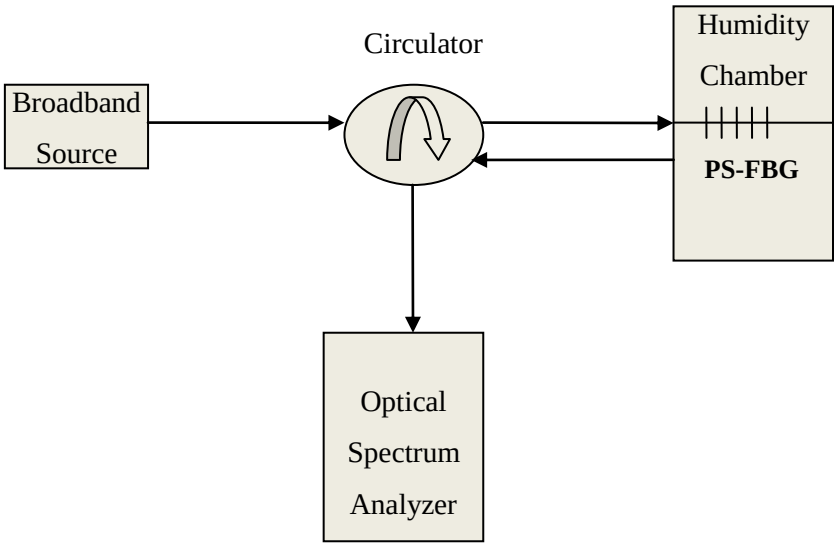

Fig. 3.7 Illustration of the experimental setup for the evaluation of PS-FBG's response to moisture

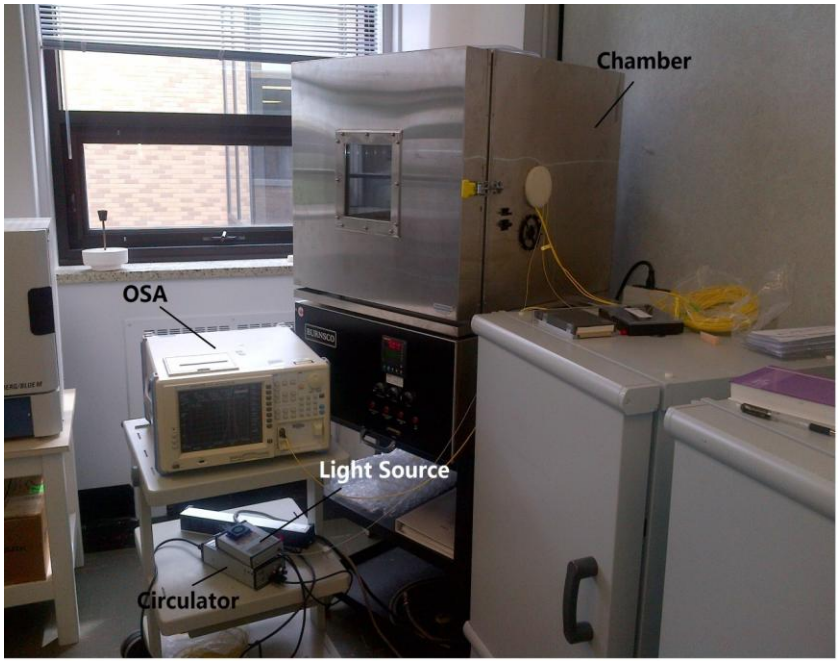

Fig. 3.8 The measurement system in the lab

Chapter 4
Results and Discussions

By using the system shown in the last chapter, some spectrums and measurement results with the humidity and temperature shift were obtained on one conventional FBG and two PS-FBGs. The major difference between these two kinds of FBG sensors is the period structure in the grating, shown as Fig. 2.6, which will lead to a sharp dip in the middle of the wavelength peak as demonstrated below.

4.1 Difference Spectrums between FBG and PS-FBG

Conventional FBGs are known for their specific wavelength peaks of reflected light, resulting from a coupling of the core modes. This specific wavelength can shift strongly with variation of environmental conditions such as humidity, temperature, pressure and strain. The property can therefore be used in the sensing system to detect such changes. However, some issues still need to be solved, particularly the measurement resolution. Since we usually measure the shift of the peak wavelength to accomplish the detection, the accurate position of the peak is crucial. Fig. 4.1 presents the typical spectra of FBG and π-PS-FBG. As shown in Fig. 4.1, it is not straightforward to distinguish the wavelength peak from the standard FBG spectrum because the peak range of the whole spectrum is flat and wide, so we cannot obtain the accurate peak wavelength value. Compared to a standard FBG sensor, with a Bragg wavelength at the center of the peak, the π-PS-FBG is split into two identical narrow peaks with a sharp divide, which can be easily observed for an accurate value, and the position of the dip is the Bragg wavelength. Therefore, using the very fine line width and sharp dip of the π-PS-FBG signal, much higher resolution and accuracy in determining the Bragg wavelength of the π-PS-FBG is possible than in the case of FBG.

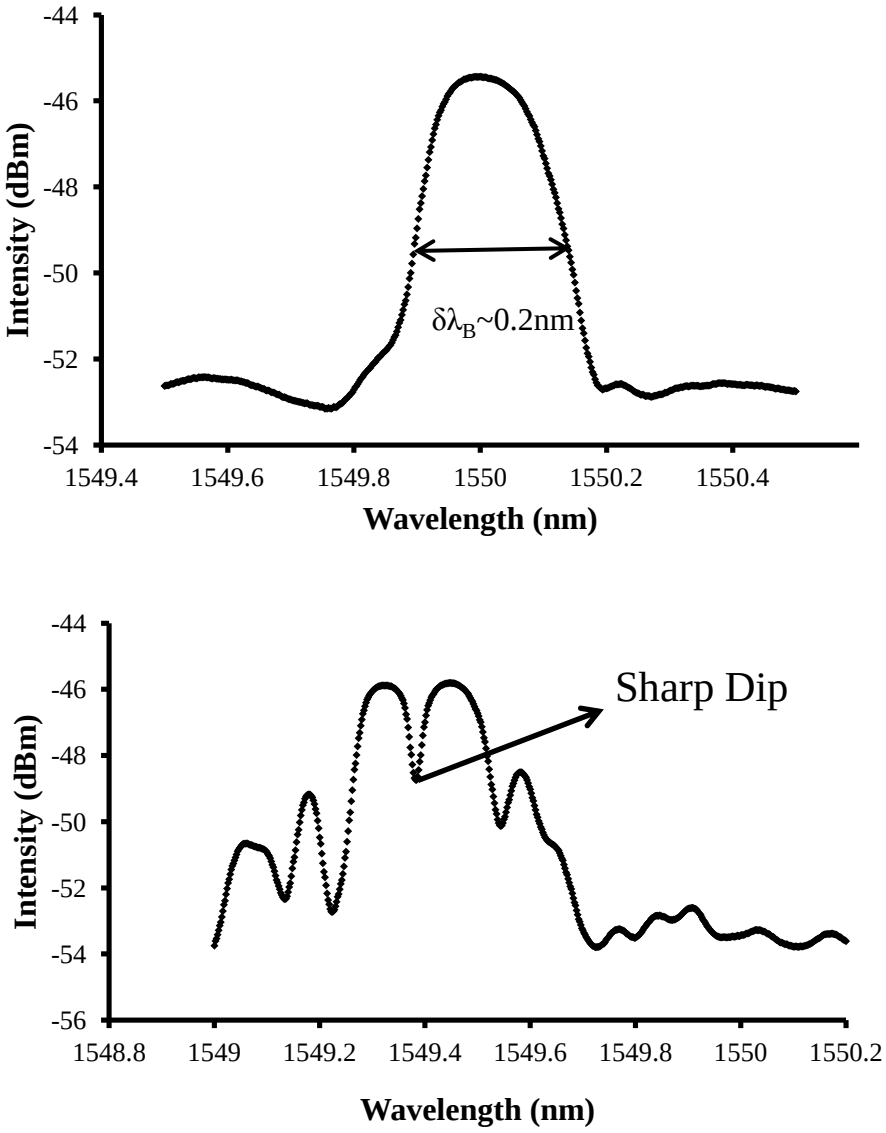

Fig. 4.1 Comparison of the spectra of standard FBG (top) and π-PS-FBG (bottom), showing a sharp dip in the bottom figure, where a more accurate wavelength value can be evaluated than from the standard FBG spectrum

4.2 Relative Humidity Response

Figure 4.2 presents a series of reflection spectra from a PS-FBG under different relative humidity at 30°C. The relative humidity is set from 10% to 90% with a 20% interval. Corresponding to the humidity sensitive property of standard FBGs, the PS-FBG also

presents a gradual increase of the Bragg wavelength resonance with different humidity levels at fixed temperature. The Bragg wavelength shifts due to the swelling of the PI coating caused by moisture absorption with increasing humidity.

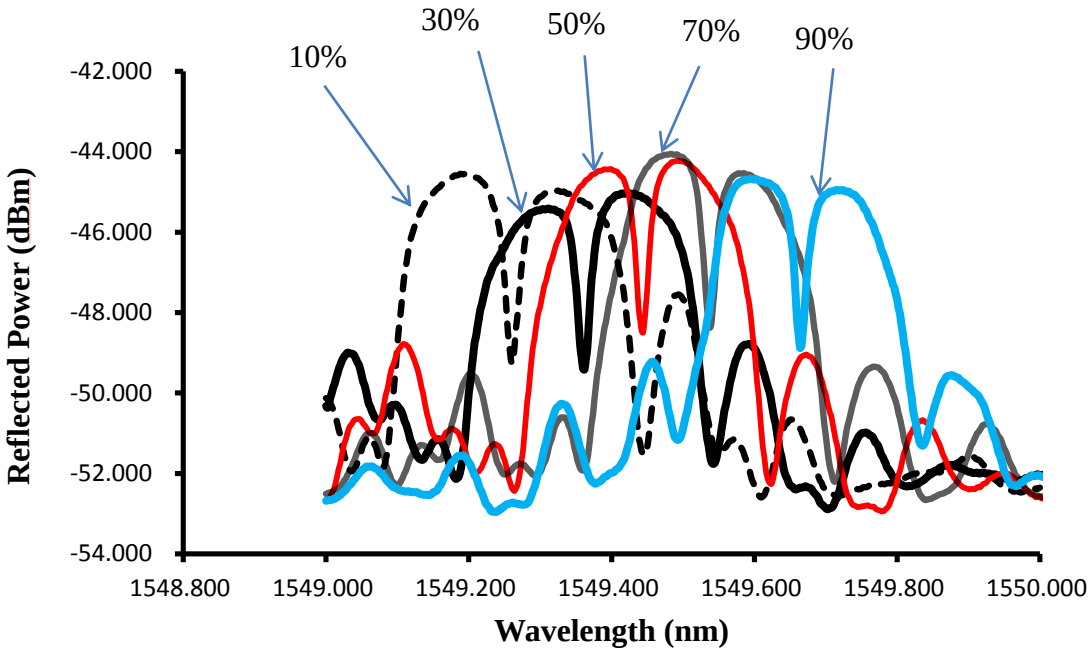

Fig. 4.2 Reflection spectra at different humidity levels (10%, 30%, 50%, 70% and 90%) at 30°C; the spectrum moves towards higher wavelength with increasing humidity.

The spectrum above presents the behavior of the FBG spectral characteristics when the sensor system was exposed to different humidity conditions. In this experiment, we use four fiber sensors, including 2 standard FBG sensors (S1 and S2) and 2 PS-FBG sensors (P1 and P2), shown in Fig. 4.3. We tested these 4 sensors at fixed temperature or humidity. Table 2 gives their diameters, which is the sum of the fiber radius and coating thickness.

	P1	P2	S1	S2
Total diameter (μm)	174.0	171.0	167.5	164

Table 2 Total radius of these four FBG sensors; the original radius of the fiber is 125 μm.

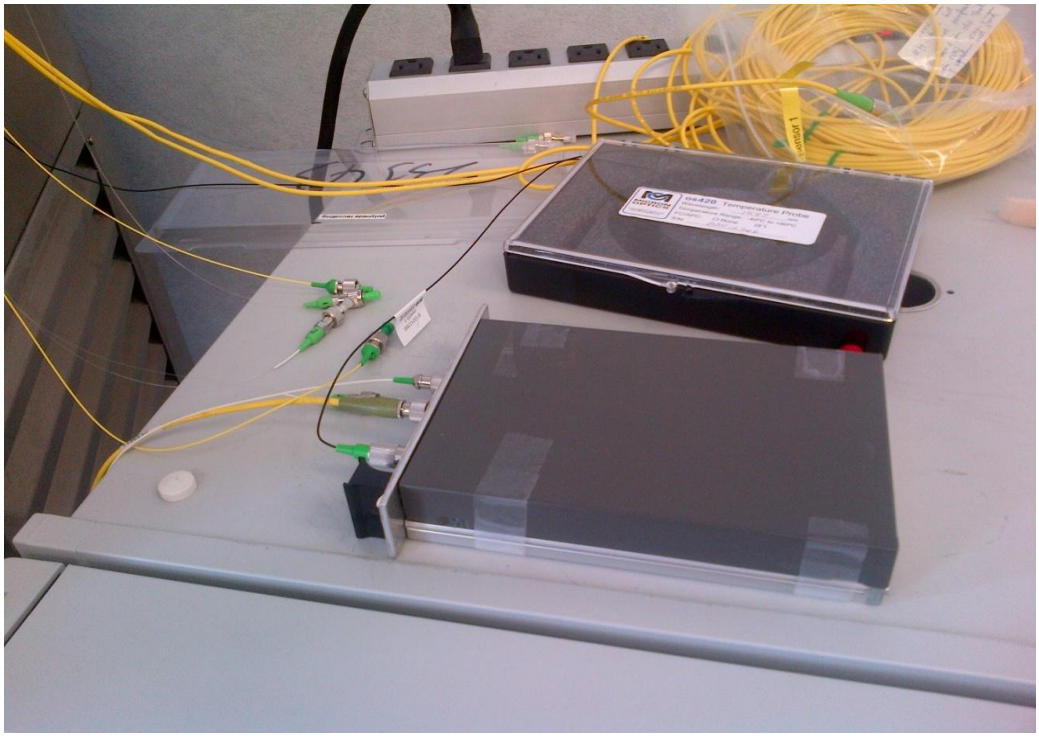

Fig. 4.3 Sensors and circulator

Sensors are kept working in the environment chamber for each 30 minute test since spectra need time to stabilize. The tests the 4 sensors shown in Fig. 4.4 and 4.5 coated with a thin PI film were measured at different humidity levels and 3 fixed temperatures. The humidity ranged from 10% to 90% with 20% intervals and the temperature was fixed at 10°C, 30°C and 50°C in each set of measurement. It is noted that the Bragg wavelength of the sensor increased linearly with the relatively humidity. Figure 4.4 and 4.5 also show that the Bragg wavelength of the π-PSFBG has a similar increase with the ambient temperature like its FBG counterparts. Moreover, their increase with ascending humidity is identical to the simulation results. Either the PS-FBG sensor or the standard FBG has a 0.2- 0.3 nm Bragg wavelength shift. Compared to the simulation results we mentioned above, with a 1 nm shift after a 3% water uptake, these shifts are larger. This could be due to that the PI coating being unable to uptake water at 3% in the humidity range of 10% to 90%. Furthermore, the value of parameters such as Young's modulus and effective photoelastic constant is temperature dependent.

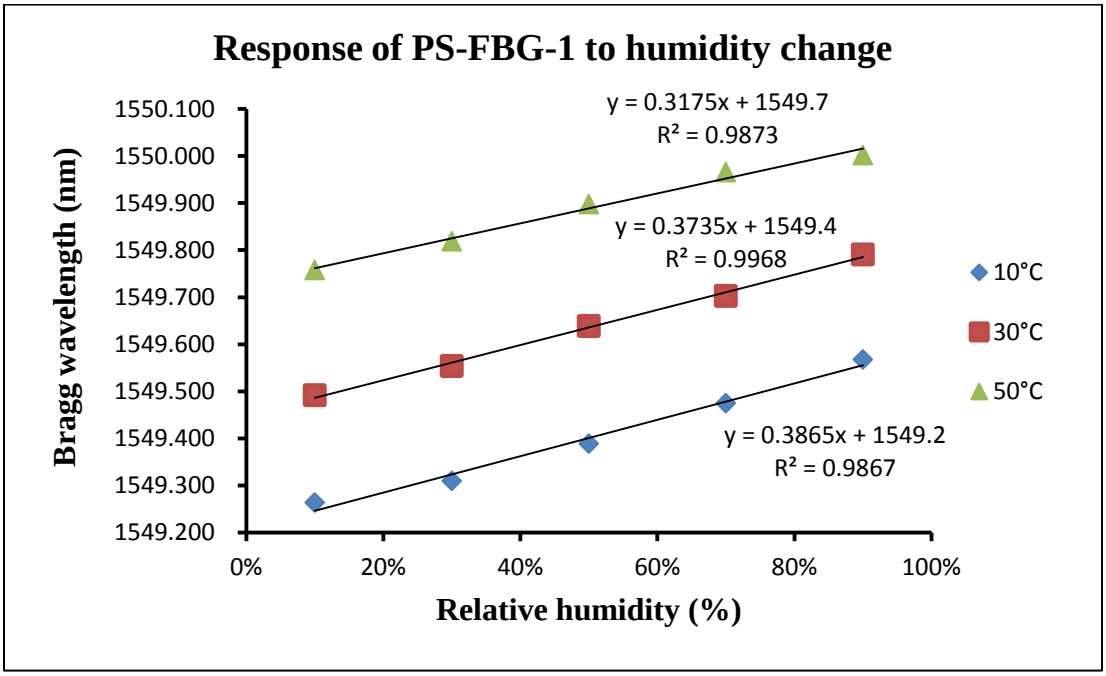

(a)

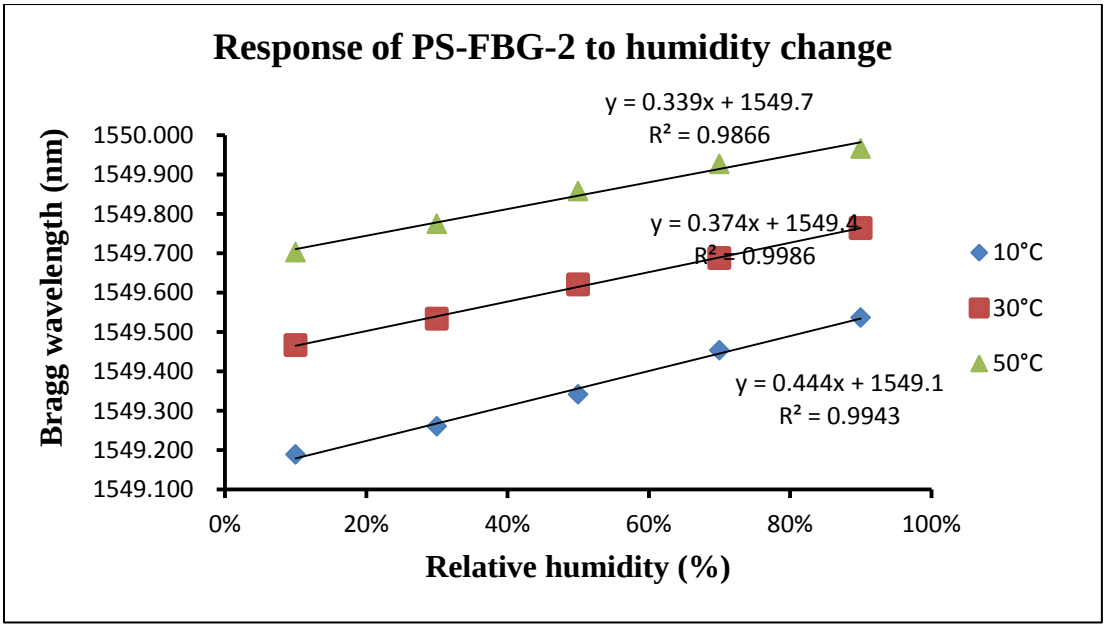

(b)

Fig. 4.4 Response of PS-FBG sensors to humidity at 10°C, 30°C and 50°C, with a humidity range of 10% to 90% (a) PS-FBG 1, (b) PS-FBG 2

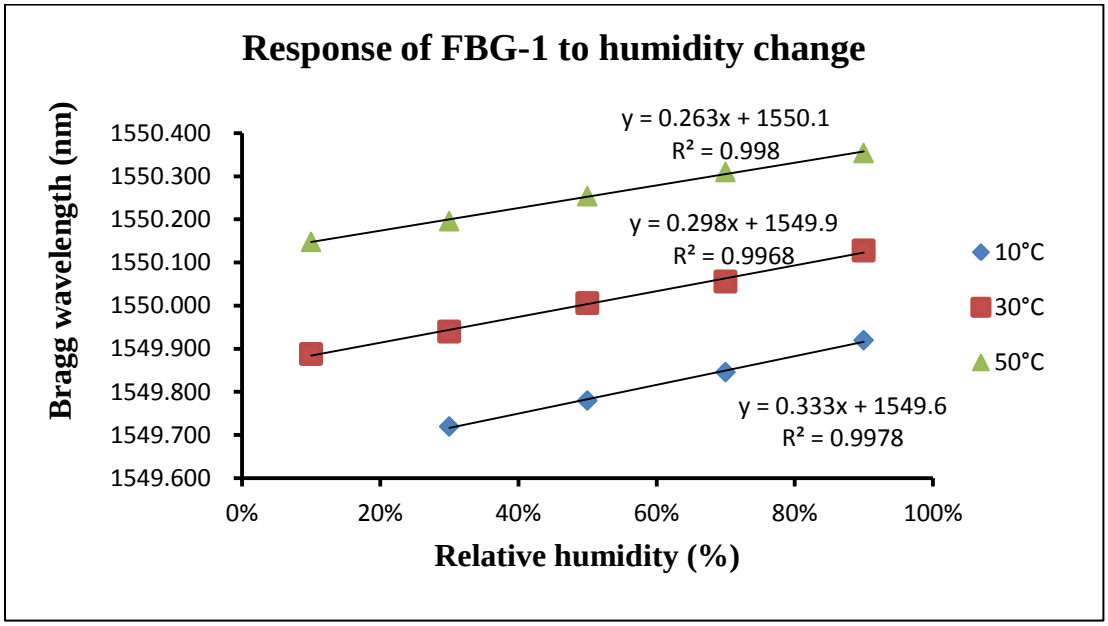

(a)

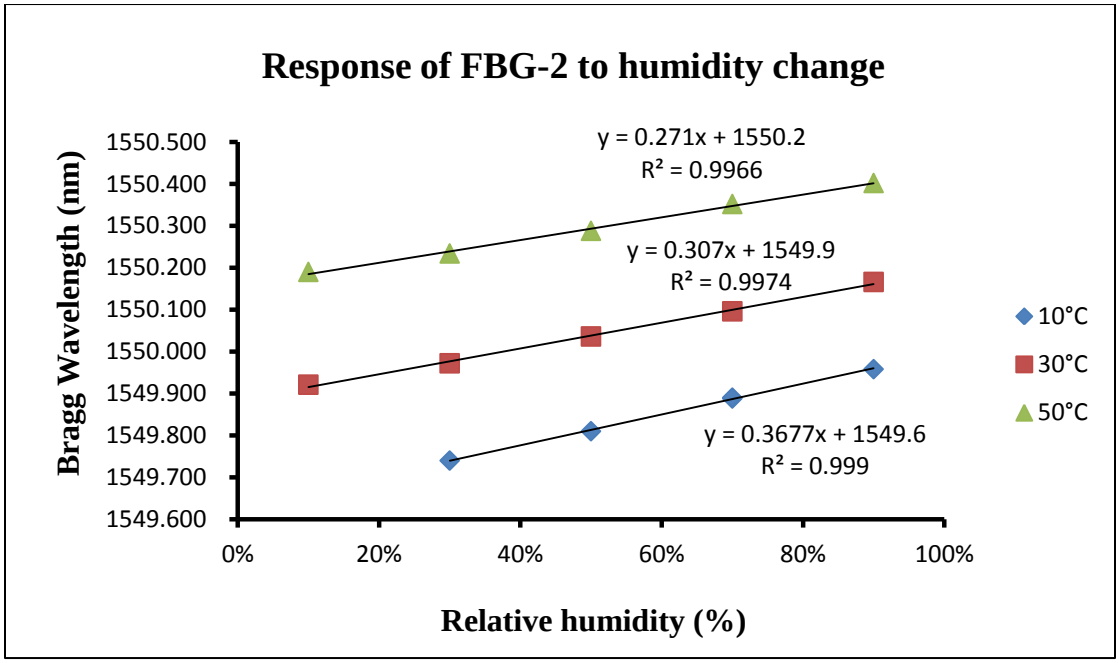

(b)

Fig. 4.5 Response of standard FBG sensors to humidity at 10°C, 30°C and 50°C, with a humidity range of 10% to 90% (a) FBG 1, (b) FBG 2

4.3 Humidity Sensitivity

Considering the relationship of the Bragg wavelength with humidity and temperature in Fig. 4.6, it is apparent that the Bragg wavelength-humidity relationship is also influenced by temperature. As shown in Fig. 3.4 (simulation), as temperature increases the sensitivity decreases for not only PS-FBG sensors but also the standard FBG sensors. Obtaining the relationship between the humidity sensitivity and the temperature as shown in Fig. 4.6, it can be seen that the highest humidity sensitivity can be achieved at lower temperature. This could be caused by the Young's modules of the PI coating decreasing with temperature. In addition, the two PS-FBGs show higher sensitivities than the standard FBG probably due to their larger thickness.

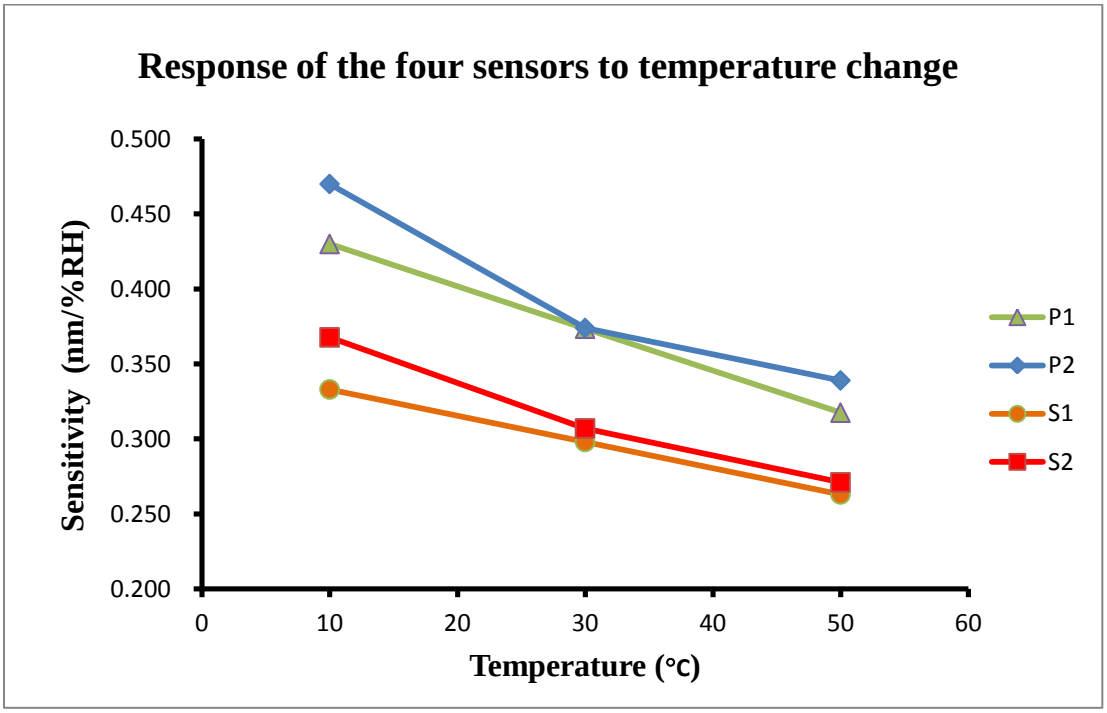

Fig. 4.6 Relationship between humidity, sensitivity and temperature, showing higher sensitivity obtained at lower temperature

4.4 Temperature Response

Besides testing these four sensors, we performed measurement of FBG sensors influenced only by temperature. The PI coating can be deformed not only by humidity

but also by a temperature change. Moreover, the temperature cross sensitivity can be simply compensated using this sensitivity relationship. The Bragg wavelength-temperature relationship (the temperature sensitivity) was reported by [51]. Figure 4.7 gives the temperature response of these four sensors. Relative humidity is fixed at 50% and temperatures range from 10 to 50 °C. Corresponding to Eq. 5, the Bragg wavelengths of both standard FBG sensors and PS-FBG sensors increase linearly with the temperature with shifts of about 0.6 nm. However, compared to the humidity response, changing temperature makes a smaller wavelength shift, which has already been demonstrated [52].

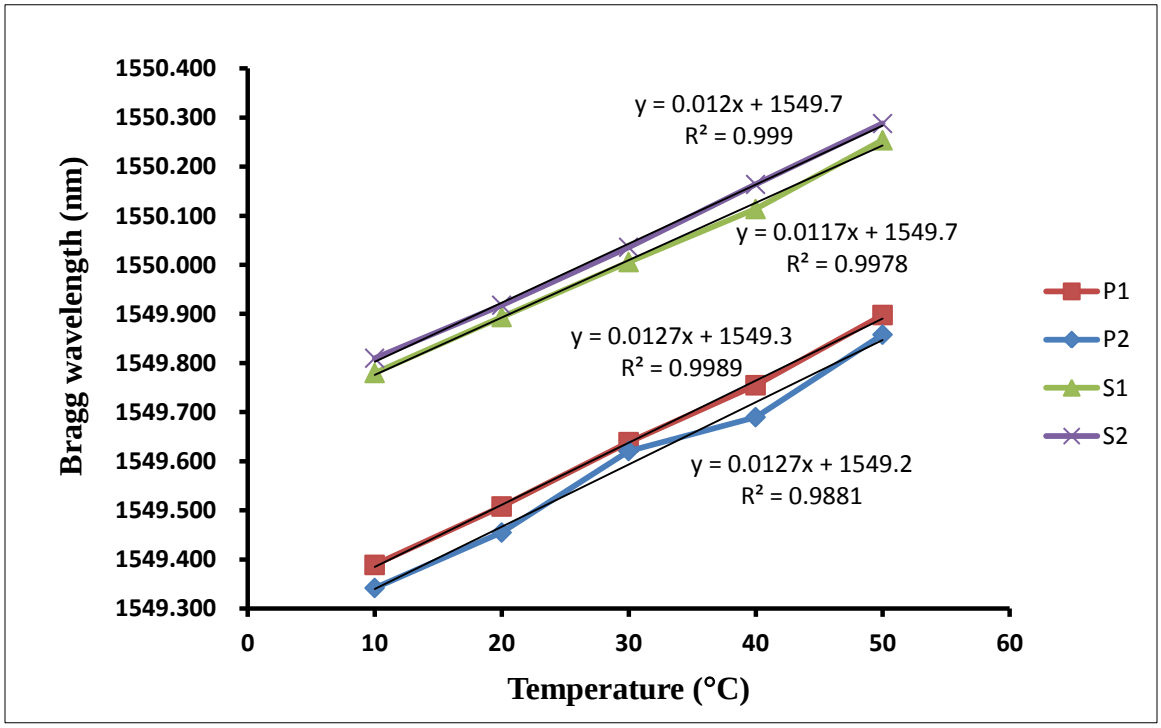

Fig. 4.7 Response of the four sensors (P1, P2, S1 and S2) to temperature change; the wavelength increases approximately linearly from 10 to 50°C

4.5 Time Response

The response time of the sensors was measure by testing them in the environmental chamber for 8 hours. The chamber is designed to allow the humidity to change from 50% to 90% and the response time is defined as the time when the wavelength shift reaches 90% of the whole average variation during the test. The response time is evaluated at a fixed

temperature of 10°C, 30°C and 50°C. For the first 3 minutes data was recorded every 30 seconds. After 3 minutes the wavelength was recorded every 3 minutes for half an hour, and then recorded every 30 minutes for 8 hours. After summarizing the data obtained in 8 hours, the PS-FBG sensor stabilized after 2 hours. The plots of the wavelength shift of S2, P1 and P2 as a function of the response time during the first 4 hours are presented in Fig. 4.8, 4.9 and 4.10, and Table 3 shows the exact response time for each sample. It can be seen that at low temperature the increase is similar to those of other temperature sets, but after 30 minutes samples still need more time to stabilize. Observing from the trend of the curves, it can be seen that the wavelength of each sensor still had a little rise after stabilizing in the ascending order (from 50%RH to 90%RH), while keeping more stable after the response time in the descending order (from 90%RH to 50%RH), due to the thermal response delay. A more rapid response occurs in the descending order from 90% to 50%, and this could result from a larger water desorption rate than absorption rate in the PI [53] [54].

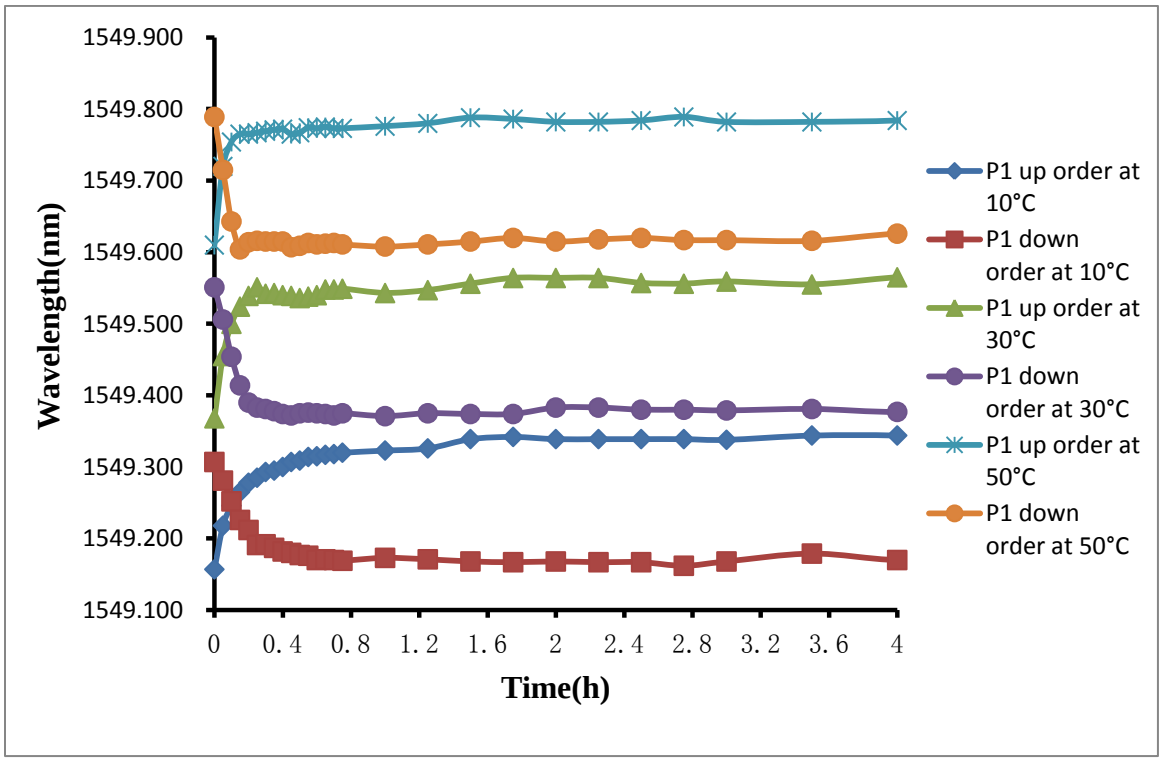

Fig. 4.8 Time response of P1 at 10°C, 30°C and 50°C during the first 4 hours

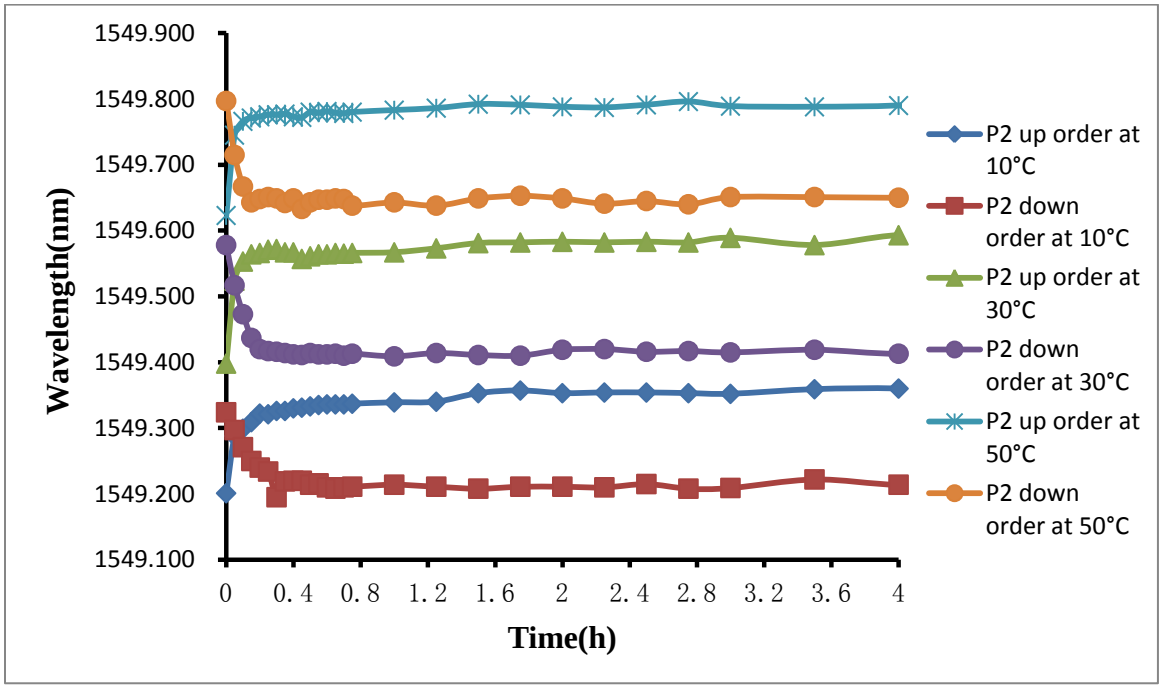

Fig. 4.9 Time response of P2 at 10°C, 30°C and 50°C during the first 4 hours

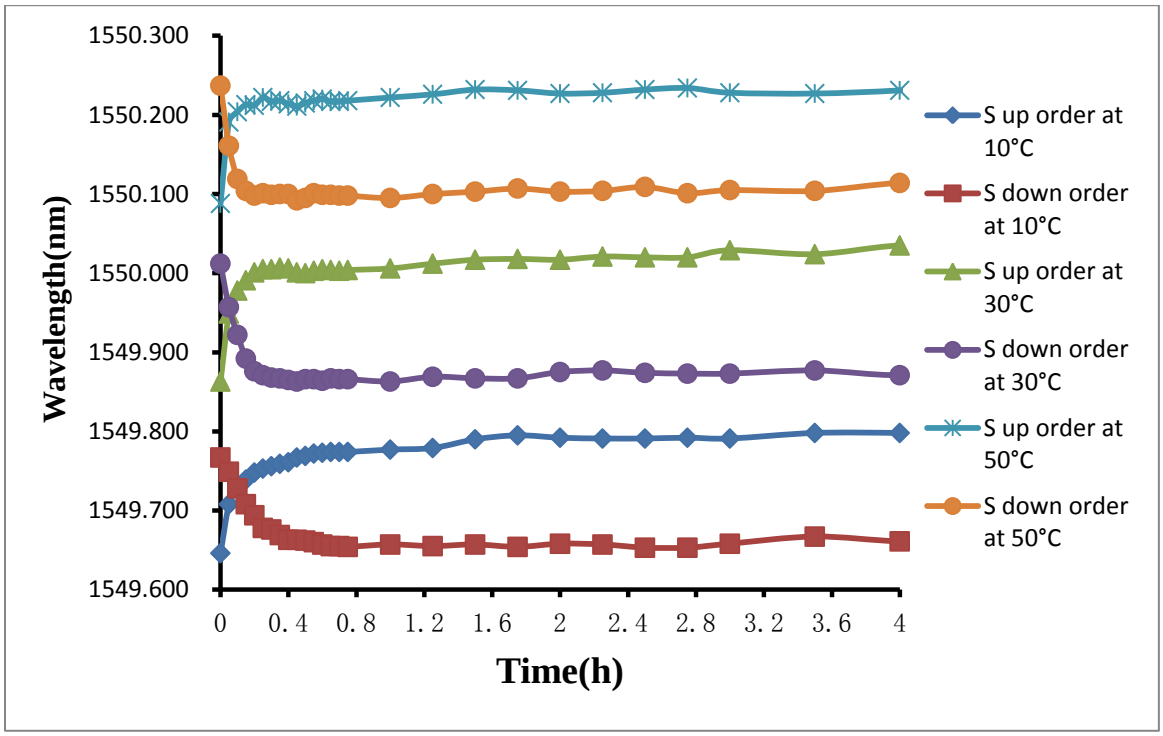

Fig. 4.10 Time response of S2 at 10°C, 30°C and 50°C during the first 4 hours

Sensor	Up(10°C)	Down(10 ℃)	Up(30 ℃)	Down(30 ℃)	Up(50 ℃)	Down(50 ℃)
P1	75	21	24	15	18	9
P2	90	18	21	12	15	9
S	90	21	24	12	18	9

Table 3 Response times of three sensors (units are in min)

4.6 Stability

To demonstrate the stability of the sensors, the humidity measurements were repeated after 7 months. We tested 3 sensors: P1, P2 and S2, Fig. 4.11 and 4.12 show the response of the three fiber sensors at temperatures of 10°C, 30°C and 50°C, with humidity varying from 40%RH to 90%RH. Comparing against the results of first test, it can be seen that the wavelength still increases approximately linearly with the humidity change and a larger range of wavelength variation is obtain, resulting in higher sensitivity for each sensor. The increasing sensitivity of each sensor can reach 1~2pm/%RH. However, unlike the trend between humidity sensitivity and temperature, Fig. 4.11 and 4.12 demonstrate that the fiber sensors show top sensitivity at 30°C instead of 10°C, as achieved by the last test. For these three sensors, tested at 10°C, the sensitivity is even lower than that of 50°C. This may be caused by the changing intrinsic properties of the PI coating exposed in the air for a long time. Good performance could not be achieved at such a low temperature.

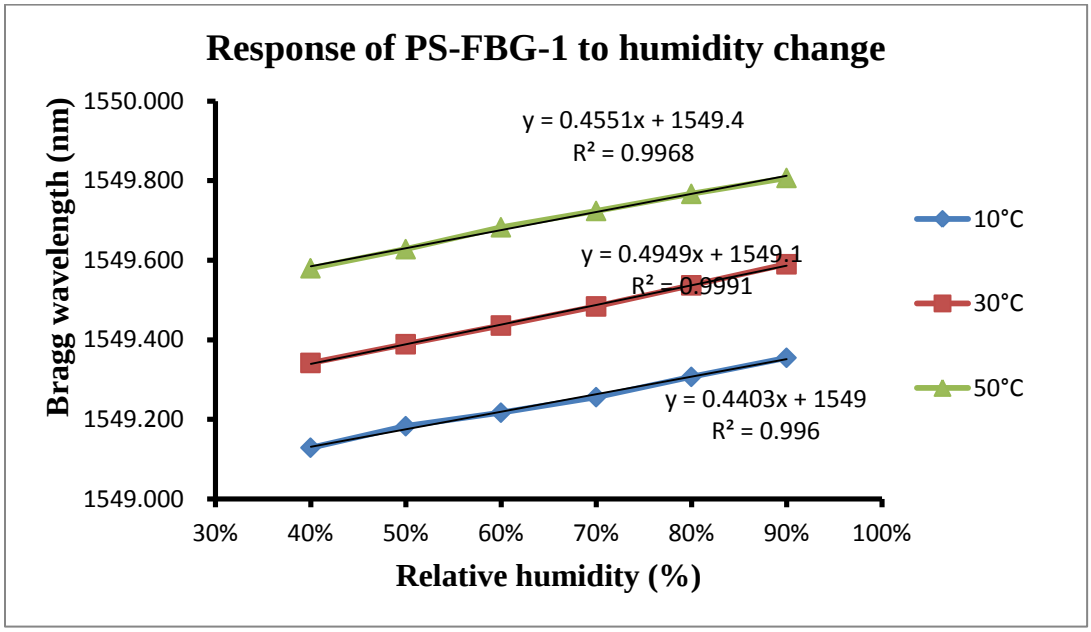

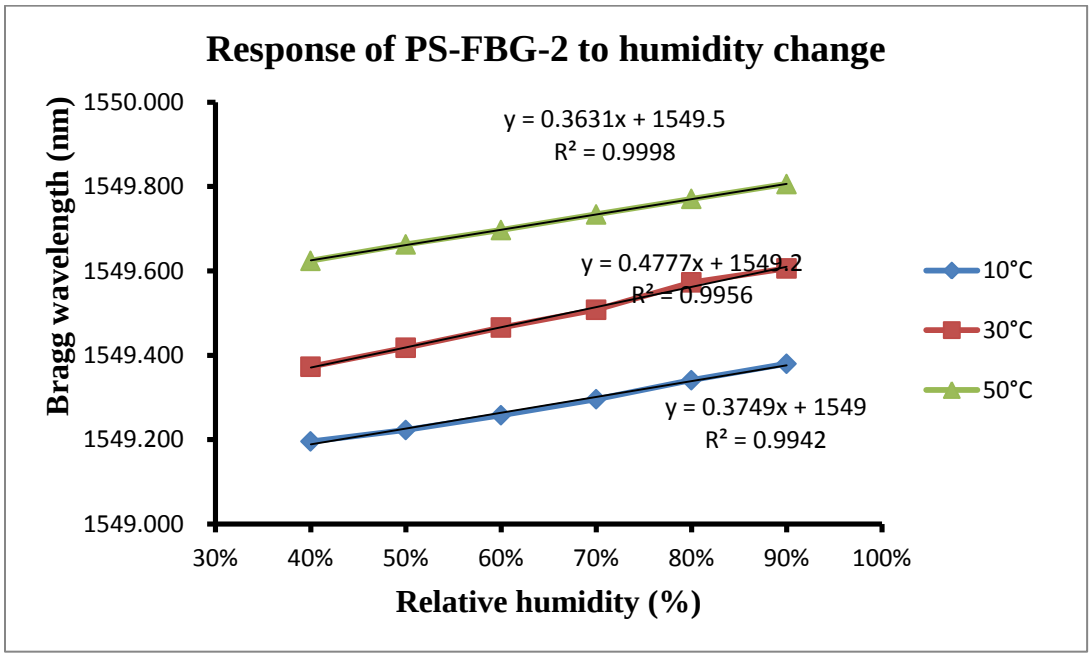

Fig. 4.11 Response of PS-FBG sensors to humidity at 10°C, 30°C and 50°C, with a humidity range of 40% to 90%

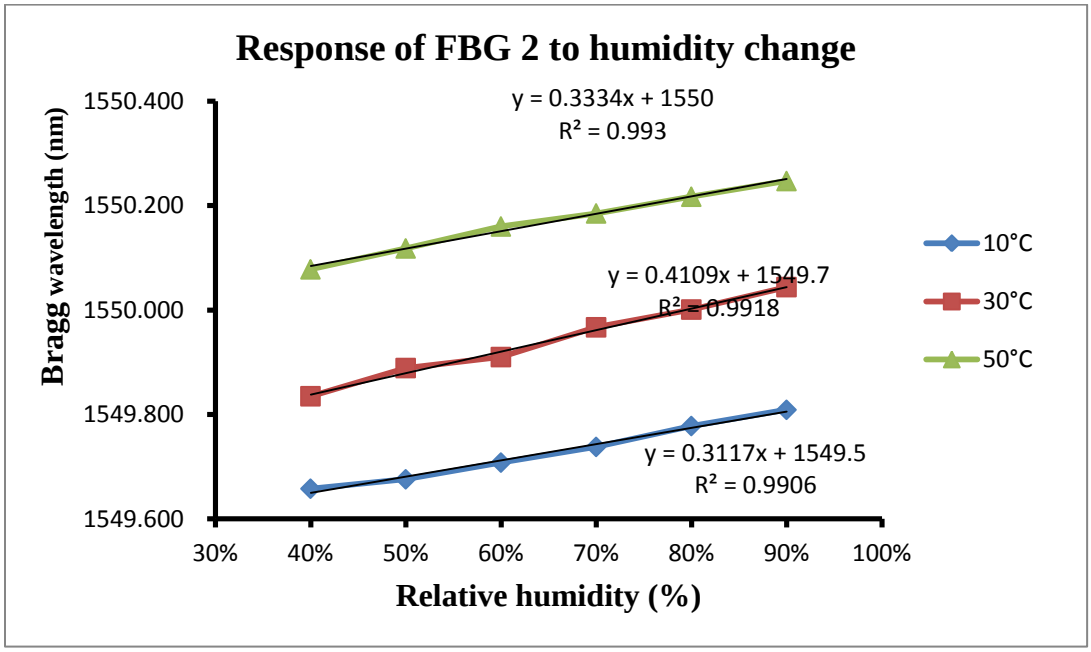

Fig. 4.12 Response of standard FBG 2 to humidity at 10°C, 30°C and 50°C, with a humidity range of 40% to 90%

Similarly, for the temperature characterization, we also repeated the temperature test. Unlike the last test, we tested the three sensors, P1, P2 and S2 in 3 sets of humidity. At the fixed temperature, Fig. 4.13 and 4.14 show the Bragg wavelength shifts in response to the temperature change in the range of 10 to 50°C with the fixed humidity at 40%RH, 60%RH and 80%RH. From the response obtained in Fig. 4.13 and 4.14, it was found that the sensitivity of each sensor to the temperature is approximately 10~12 pm/°C. With the increasing humidity the Bragg wavelength increases due to temperature sensing of the PI. Comparing PS-FBG with the standard FBG, the plots show similar trends for each sets of value, leading to the comparable function in temperature sensing for PS-FBG sensors.

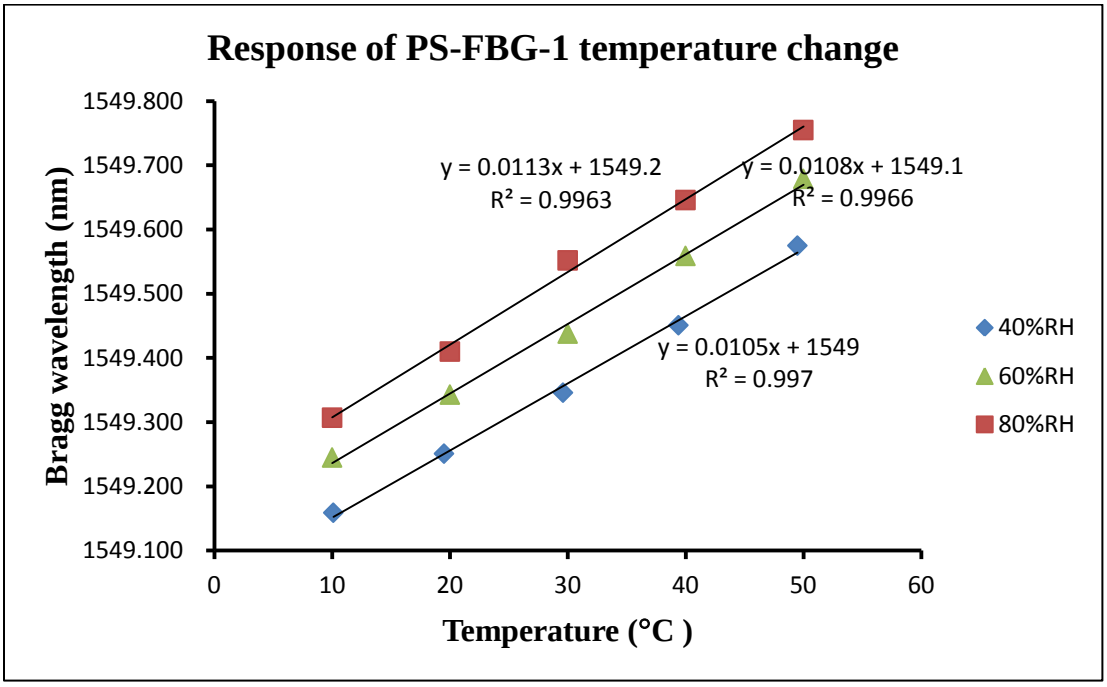

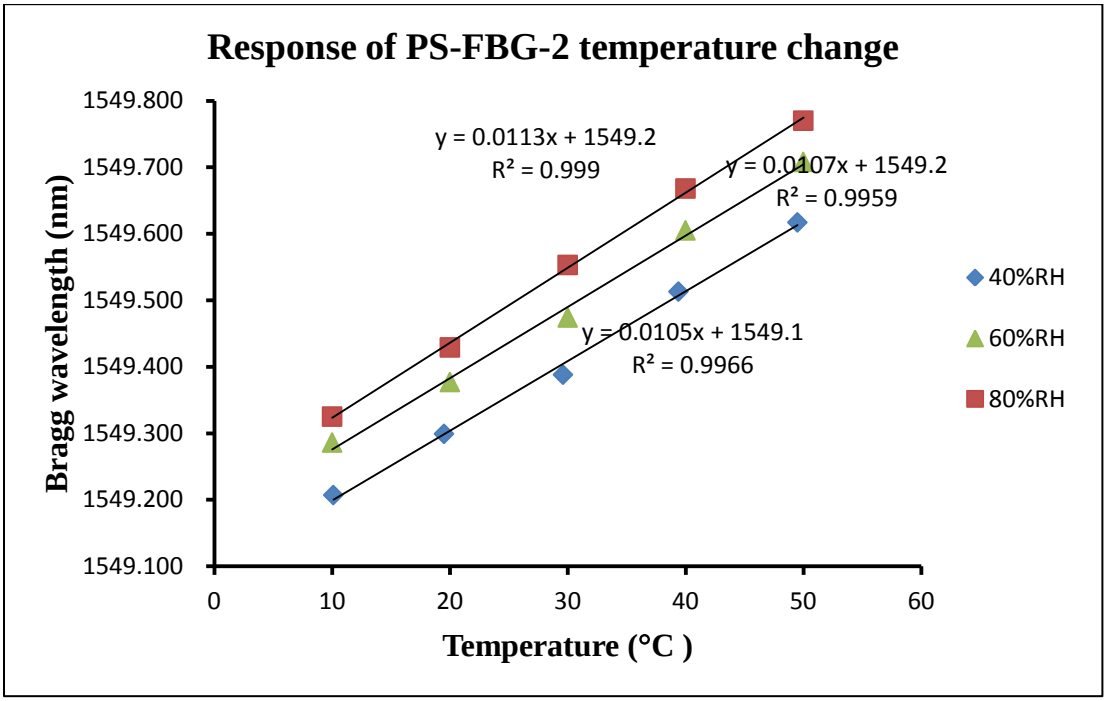

Fig. 4.13 Response of PS-FBG sensors to temperature at 40%, 60% and 80%RH, with a temperature range of 10 to 50°C

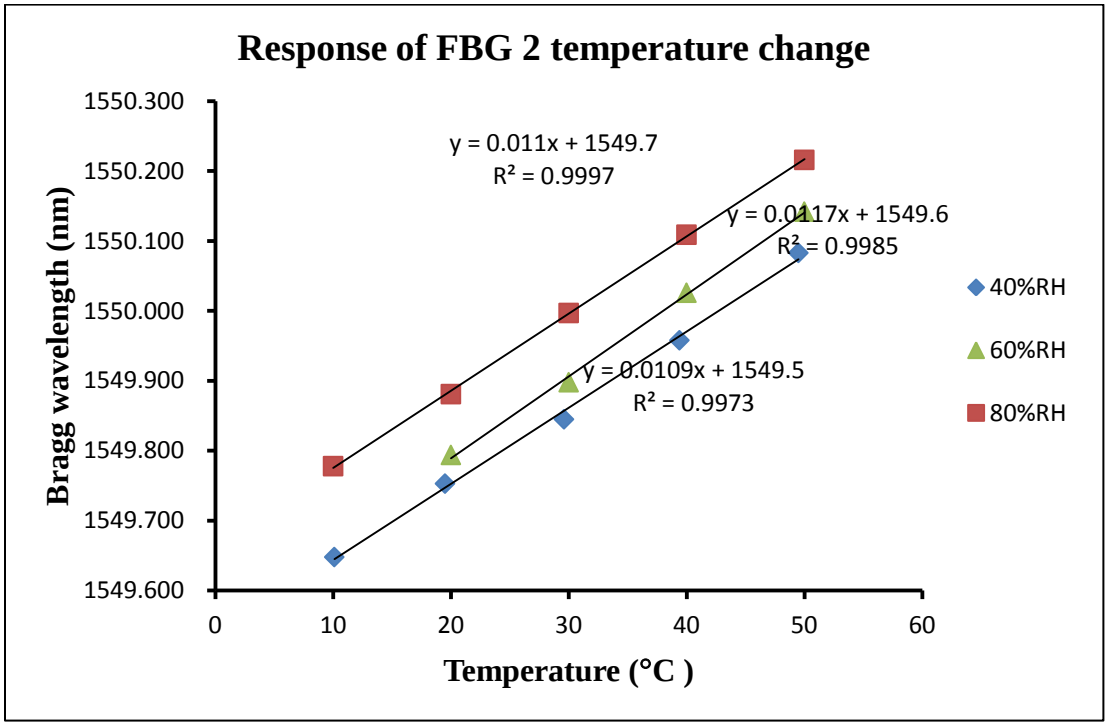

Fig. 4.14Response of standard FBG 2 sensors to temperature at 40%, 60% and 80%RH, with a temperature range of 10 to 50°C

4.7 Hysteresis

Hysteresis of a FBG sensor is a parameter showing the performance not only during its ascending order but also during descent. The hysteresis characteristics of these three sensors in the two experiments were also tested. As shown in Fig. 4.15, the temperature is fixed at 30°C and the hysteresis of the full measurement range is mostly within 15%, which is bigger than that of other results [55]. In fact, the hysteresis should be controlled within 5% [56] to achieve a good FBG sensor. It can be easily seen that the sensors shows a smaller hysteresis under higher humidity. Thus, the hysteresis is another parameter that needs to be improved.

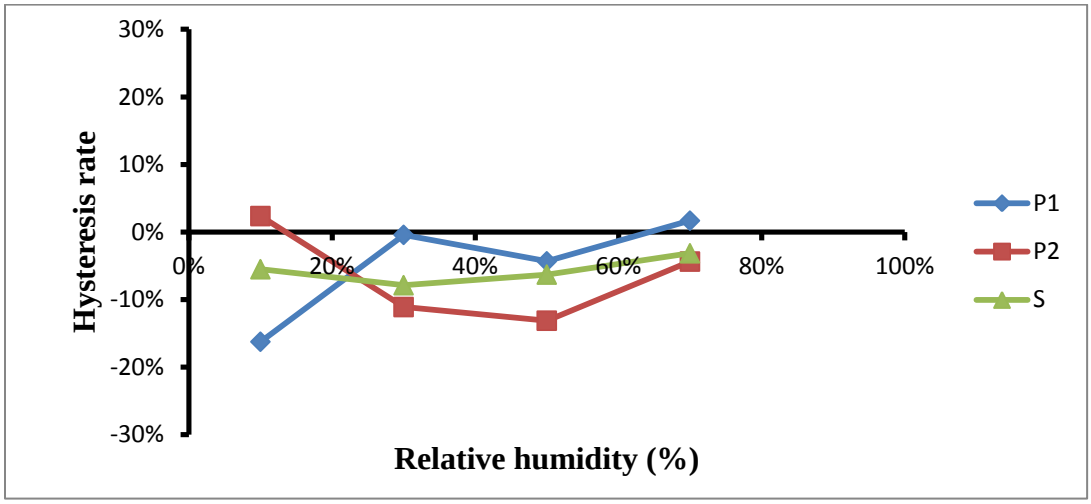

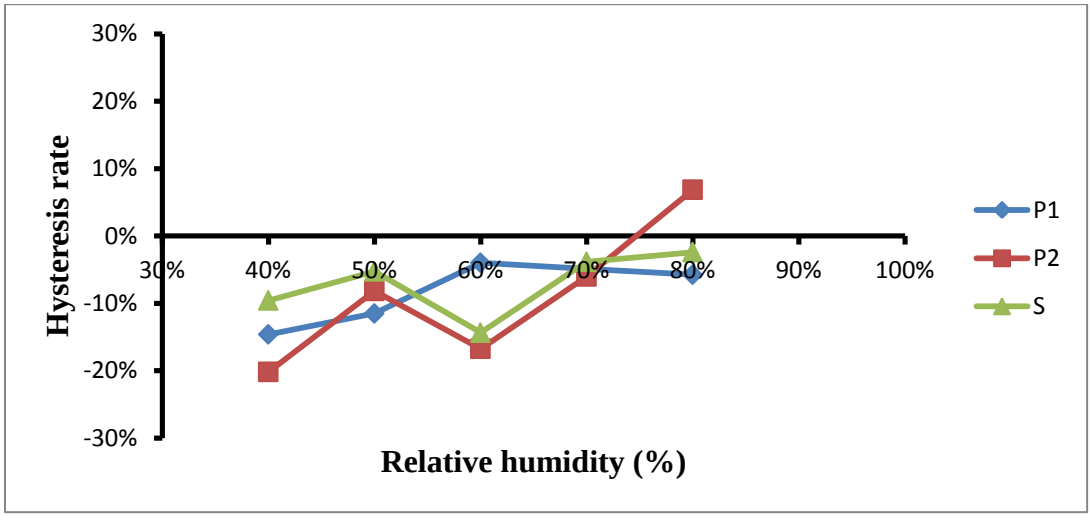

Fig. 4.15 Hysteresis of the two measurements

Chapter 5
Conclusion

In this research, we have presents a new method to measure the temperature and humidity with phase-shifted fiber Bragg grating sensors. We characterized of humidity sensors based on a standard FBG and a π-PS-FBG, testing resolution, sensitivity, response time and hysteresis. The PS-FBG can produce a sharper dip in contrast to the flat peak in a standard FBG spectrum, leading to a narrow 3dBm bandwidth. Achieving higher resolution means we can identify temperature and humidity changes with greater sensitivity and efficiency.

We modeled the relationship between the wavelength shift and water uptake, fiber radius, coating thickness and humidity, respectively, and numerically simulated the time response. In the experiments we measured 4 samples, 2 standard FBGs (S1 and S2) and 2 PS-FBGs (P1 and P2) in different conditions. It was found that the Bragg wavelength of the sensor increases linearly with both the ambient humidity and temperature, and the sensitivity of each sensor can reach 2.5-4.5pm/% for the humidity response and 10~12 pm/°C for the temperature response. It was also found that the humidity sensitivity of the sensor decreases with ambient temperature. With the narrow bandwidth, PS-FBGs gave a higher resolution than standard FBGs and allowed acquisition of wavelength in the sub-pm level, and they have similar response trends to humidity and temperature as standard FBGs. Moreover, the response times of P1, P2 and S2 are illustrated in the last chapter, shown in Table 3. They are limited to 30 minutes at 30°C and 50°C while the response time is over 1 hour at 10°C. We also analyzed the stability and hysteresis, which were inferior to devices demonstrated in other references, demanding future improvement.

This work shows the basic concepts and measurements involved in using PS-FBG sensors. However, there are still some challenges which need to be considered, such as the sensitivity, stability and hysteresis. Further work is also envisaged to explore the use of such sensors and other sensors with different coatings in order to enhance the

sensitivity and lower the response time. In addition, these devices can also be applied in the measurement of strain, pressure and solution concentration.

References

1. P. Tsai, F. Sun, G. i Xiao, Z. Zhang, S. Rahimi , and Dayan Ban, "A New Fiber-Bragg-Grating Sensor Interrogation System Deploying Free-Spectral-Range-Matching Scheme With High Precision and Fast Detection Rate," IEEE Photon. Technol. Lett., Vol. 20, No. 4, Feb. 15, 2008

2. G. Xiao, N. Mrad, F. Wu, Z. Zhang and F. Sun, "Miniaturized optical fiber sensor interrogation system employing echelle diffractive gratings demultiplexer for potential aerospace applications", IEEE Sens. J. Vol. 8, pp. 1202-1207, 2008

3. H. Guo, G. Xiao, N. Mrad and J. Yao, "Static and dynamic strain fiber Bragg grating sensor interrogation using a monolithically integrated echelle diffractive grating", In Proceedings of 21st International Conference on Optical Fiber Sensors, edited by Wojtek J. Bock, Jacques Albert, Xiaoyi Bao, Proc. of SPIE Vol. 7753, 775379, 2011

4. P. Kronenberg, P. K. Rastogi, P. Giaccari and H. G. Limberger, "Relative humidity sensor with optical fiber Bragg gratings", Optic. Lett. Vol. 27, pp. 1385-1387, 2002

5. T. L. Yeo, T. Sun, K. T. V. Grattan, D. Parry, R. Lade and B. D. Powell, "Polymer-coated fiber Bragg grating for relative humidity sensing", IEEE Sensors J., Vol. 5, pp. 1082-1089, 2005

6. D. C. Betz, G. Thursby, B. Culshaw, W. J. Staszewski, "Acousto-ultrasonics sensing using fiber Bragg grating", Smart Mater. Struct. Vol. 12, pp. 122-128, 2003

7. G. Wild, S. Hinckley, "Acousto-Ultrasonic optical fiber sensors: Overview and state-of-the-art", IEEE Sens. J. Vol. 8, 1184-1193, 2008

8. Qi Zhang, Nan Liu, Thomas Fink, Hong Li, Wei Peng, and Ming Han , "Fiber-Optic Pressure Sensor Based on π-Phase-Shifted Fiber Bragg Grating on Side-Hole Fiber," IEEE Photonics Technology Letters, Vol. 24, No. 17, September 1, 2012

9. Bal, Harpreet K., Sidiroglou, Fotios, Brodzeli, Zourab, Wade, Scott A., Baxter, Greg W., Collins, Stephen F., "Temperature independent bend measurement using a pi-

phase shifted FBG at twice the Bragg wavelength," Proc. SPIE 7653, 76530H (1-4), 2012

10. Sui P. Yam, Zourab Brodzeli, Betty P. Kouskousis, Claire M. Rollinson, Scott A. Wade, Greg W. Baxter,1 and Stephen F. Collins, "Fabrication of a π-phase-shifted fiber Bragg grating at twice the Bragg wavelength with the standard phase mask technique," Optics letters, Vol:34, No:13, 2021 -2023 (2009)
11. Bal, Harpreet K.; Dragomir, Nicoleta M.; Sidiroglou, Fotios; Wade, Scott A.; Baxter, Greg W.; Collins, Stephen F., "Response of some pi-phase-shifted Bragg gratings to elevated pressure", Proceedings of SPIE - The International Society for Optical Engineering, v 7753, 2011
12. Sui P. Yam, Zourab Brodzeli, Betty P. Kouskousis, Claire M. Rollinson, Scott A. Wade, Greg W. Baxter,1 and Stephen F. Collins,"Fabrication of a π-phase-shifted fiber Bragg grating at twice the Bragg wavelength with the standard phase mask technique," Optics letters, vol:34, no:13, pp 2021 -2023, 2009
13. Meltz, G., Morey, W.W.; Glenn, W.H., "Formation of Bragg gratings in optical fibers by a transverse holographic method", Optics letters, Vol:14 Iss:15 Pg:823 -5, 1989
14. Arregui, Francisco J.; Matías, Ignacio R.; Cooper, Kristie L.; Claus, Richard O., "Simultaneous measurement of humidity and temperature by combining a reflective intensity-based optical fiber sensor and a fiber bragg grating", IEEE Sensors Journal, v 2, n 5, p 482-487, 2002
15. T. Li, X. Dong, C. Chan, C. Zhao, and Peng Zu, " Humidity Sensor Based on a Multimode-Fiber," IEEE Sensors Journal, Vol. 12, No. 6, June 2012
16. Gwo-Shyang Hwang; Chien-Ching Ma; Ding-Wei Huang; Liang Liao, "Study on reflection spectrum areas of an FBG for strain gradient measurements, ", IEEE Sensors, p 4 pp., 2012

17. Yao, Yuan ; Zhou, Ciming; Wang, Dongli; Wu, Lin, "Research on fiber Bragg grating huge current sensing based on electromagnetic force" Proceedings of SPIE - The International Society for Optical Engineering, v 8191, 2011

18. Sengupta, D. ; Sai Shankar, M.; Saidi Reddy, P.; Sai Prasad, R.L.N.; Srimannarayana, K. , "An FBG based hydrostatic pressure sensor for liquid level measurements", Proceedings of SPIE - The International Society for Optical Engineering, v 8426, 2012

19. Arasu, P.T.; Al-Qazwini, Y.; Onn, B.I.; Noor, A.S.M. , "Fiber Bragg grating based surface plasmon resonance sensor utilizing FDTD for alcohol detection applications", 2012 IEEE 3rd International Conference on Photonics (ICP 2012), p 93-7, 2012

20. Bai, Junjie; Zhao, Damei; Zhang, Xiuyan , "Structural health monitoring of smart civil structures based on fiber Bragg grating sensing technology", 2011 2nd International Conference on Artificial Intelligence, Management Science and Electronic Commerce, AIMSEC 2011 - Proceedings, p 635-638, 2011

21. Gao, Junqi; Wu, Jin; Li, Jun; Zhao, Xinming, "Monitoring of corrosion in reinforced concrete structure using Bragg grating sensing", Source:NDT and E International, v 44, n 2, p 202-205, March 2011

22. Sun, Li; Zhang, Haixia; Liang, Dezhi; Li, Zhe, "Application of FBG sensors in shaking table test of frame-shear wall structure mode", Advanced Materials Research, v 163-167, p 2653-2656, 2011

23. Willsch, M. ; Bosselmann, T.; Villnow, M.; Ecke, W. "Fiber optical sensor trends in the energy field", Proceedings of SPIE - The International Society for Optical Engineering, v 8421, 2012

24. G. Xiao, N. Mrad, F. Wu, Z. Zhang and F. Sun, "Miniaturized optical fiber sensor interrogation system employing echelle diffractive gratings demultiplexer for potential aerospace applications", IEEE Sens. J. Vol. 8, pp. 1202-1207, 2008

25. Poeggel, Sven; Leen, Gabriel; Bremer, Kort; Lewis, Elfed "Miniature Optical fiber combined pressure- and temperature sensor for medical applications", Proceedings of IEEE Sensors,2012

26. Liu, Kun; Liu, Tiegen; Jiang, Junfeng; Jing, Wencai; Wang, Yan; Zhang, Hongxia; Jia, Dagong; Zhang, Yimo, "Research of hybrid fiber physical and chemical sensing system", Zhongguo Jiguang/Chinese Journal of Lasers, v 36, n SUPPL. 2, p 299-305, December 2009

27. Byoungho Lee, "Review of the present status of optical fiber sensors", Optical Fiber Technology: Materials, Devices and Systems, v 9, n 2, p 57-79, April 2003

28. Filograno, M.L.; Corredera Guillen, P.; Rodriguez-Barrios, A.; Martin-Lopez, S.; Rodriguez-Plaza, M.; Andres-Alguacil, A.; Gonzalez-Herraez, M, "Real-Time Monitoring of Railway Traffic Using Fiber Bragg Grating Sensors", IEEE Sensors Journal, v 12, n 1, p 85-92, Jan. 2012

29. Fiebrandt, J.; Leich, M.; Rothhardt, M.; Bartelt, H., I"n-fiber temperature measurement during optical pumping of Yb-doped laser fibers", Proceedings of the SPIE - The International Society for Optical Engineering, v 8426, p 84260B (8 pp.), 2012

30. Carmo, J.P.; da Silva, A.M.F.; Rocha, R.P.; Correia, J.H. "Application of Fiber Bragg Gratings to Wearable Garments", IEEE Sensors Journal, v 12, n 1, p 261-6, Jan. 2012

31. Li, Hongqiang; Li, Yang; Li, Enbang; Dong, Xiaye; Bai, Yaoting; Liu, Yu; Zhou, Wenqian , "Temperature-insensitive arrayed waveguide grating demodulation technique for fiber Bragg grating sensors", Optics and Laser Technology, v 51, p 77-81, 2013

32. Ou Xu; Shaohua Lu; Suchun Feng; Zhongwei Tan; Tigang Ning; Shuisheng Jian, "Single-longitudinal-mode erbium-doped fiber laser with the fiber-Bragg-grating-

based asymmetric two-cavity structure", Optics Communications, v 282, n 5, p 962-5, 1 March 2009

33. P. Kronenberg, P. K. Rastogi, P. Giaccari, and H. G. Limberger, "Relative humidity sensor with optical fiber Bragg grating," Opt. Lett., vol. 27, pp. 1385–1387, 2002
34. W. Zhang, D. J. Webb and G.-D. Peng , "Improved time response for polymer fibre Bragg grating based humidity sensors," Proceedings of SPIE--the international society for optical engineering, vol:7753, 2011
35. Pascal Kronenberg, Pramod K. Rastogi, Philippe Giaccari and Hans G. Limberger , "Relative humidity sensor with optical fiber Bragg gratings," Optics Letters, Vol. 27, No. 16, August 15, 2002
36. Sui P. Yam, Zourab Brodzeli, Betty P. Kouskousis, Claire M. Rollinson, Scott A. Wade, Greg W. Baxter,1 and Stephen F. Collins, "Fabrication of a π-phase-shifted fiber Bragg grating at twice the Bragg wavelength with the standard phase mask technique," Optics letters, Vol:34, No:13, 2021 -2023 (2009)
37. Lipson, S.G.; Lipson, H.; Tannhauser, D.S. (1995). Optical Physics (3rd ed.). London: Cambridge U.P. p. 248
38. D. Gatti, G. Galzerano, D. Janner, S. Longhi and P. Laporta, "Fiber strain sensor based on a π-phase-shifted Bragg grating and the Pound-Drever-Hall technique", Optic. Express, Vol. 16, pp. 1945-1950, 2008
39. T. Liu and M. Han, "Analysis of π-phase-shifted fiber bragg gratings for ultrasonic detection", IEEE Sensors J., Vol. 12, pp. 2368-2373, 2012
40. A. I. Azmi, D. Sen, W. Sheng, J. Canning and G.-D. Peng, "Performance enhancement of vibration sensing employing multiple phase-shifted fiber Bragg grating", IEEE/OSA J. Lightwave Technol., Vol. 29, pp. 3453-3460, 2011
41. Zhang, Qi; Liu, Nan; Fink, Thomas; Li, Hong; Peng, Wei; Han, Ming "Fiber-optic pressure sensor based on π-phase-shifted fiber Bragg grating on side-hole fiber", IEEE Photonics Technology Letters, v 24, n 17, p 1519-1522, 2012

42. C. Martinez and P. Ferdinand, “Analysis of phase-shifted fiber Bragg gratings written with phase plates,” APPLIED OPTICS, Vol. 38, No. 15, 3223 -3228 (1999)

43. M. Torn, A. Shibuya and K. Takemura, “Reliability of polyimide-based thin and flexible capacitors with SrTiO3”, Proceedings of 9th IEEE VLSI Packaging Workshop of Japan, pp. 131-134, 2008

44. P. Kronenberg, P. K. Rastogi, P. Giaccari, and H. G. Limberger, “Relative humidity sensor with optical fiber Bragg grating,” Opt. Lett., vol. 27, 1385–1387 (2002).

45. PI-2525_2555_2556_2574_ProductBulletin, HD MicroSystems, 2009

46. T.L. Yeo, T. Sun, K.T.V. Grattan, D. Parry, R. Lade, B.D. Powell, “Characterisation of a polymer-coated fibre Bragg grating sensor for relative humidity sensing,” Sensors and Actuators B 110 (2005) 148–155

47. Teck L. Yeo, Tong Sun, Kenneth T. V. Grattan, David Parry, Rob Lade, and Brian D. Powell , “Polymer-Coated Fiber Bragg Grating for Relative Humidity Sensing,” IEEE Sensors Journal, Vol. 5, No. 5, Oct. 2005

48. F. Y. Tsai, T. N. Blanton, D. R. Harding, and S. H. Chen, “Temperature dependence of the properties of vapor-deposited polyimide”, Journal of Applied Physics, Vol. 93, n 7, p 3760-4, 1 April 2003

49. Peeyush Bhargava, Kathy C. Chuang, Kenway Chen, Alan Zehnder, “Moisture Diffusion Properties of HFPE-II-52 Polyimide”, Journal of Applied Polymer Science Vol. 102, pp.3471-3479, 2006

50. Haitao Qi; Jiaguo Liu “Time-fractional radial diffusion in hollow geometries”, Meccanica, v 45, n 4, p 577-583, August 2010

51. D. T. Turner, “Polymethyl methacrylate plus water: Sorption kinetics and volumetric changes,” Polymer, vol. 23, pp. 197–202, 1982

52. A. G. Thomas and K. Muniandy, “Absorption and desorption of water in rubbers,” Polymer, vol. 28, pp. 408–415, 1987